Tsinghua Science and Technology
Doi:10.26599/TST.2026.9010059

Research

A Level-Direction Guided Hierarchical Particle Swarm Optimization for Wind Farm Layout Optimization

Tao Zheng, Sichen Tao, Wenzhu Gu, Zhenyu Lei, and Shangce Gao (✉)

Abstract Wind Farm Layout Optimization Problem (WFLOP) aims to optimize turbine placement to mitigate wake-effect losses and improve power generation efficiency. Existing particle swarm optimization (PSO)-based approaches for WFLOP mainly rely on conventional variants and lack problem-specific search mechanisms. To address this limitation, this paper proposes a level-direction guided hierarchical particle swarm optimization algorithm (HGPSO). The proposed method integrates multi-direction guidance and hierarchical learning to enhance population diversity and convergence performance. Comprehensive experiments under various wind conditions, turbine scales, and land constraints show that HGPSO outperforms several state-of-the-art WFLOP optimizers in most test cases, achieving average improvements of approximately 0.5%–3.0% in energy conversion efficiency. Statistical tests further confirm its robustness and stability. The proposed HGPSO provides an effective and scalable solution for complex wind farm layout optimization.

Keywords Wind farm layout optimization problem, Level-direction guided hierarchical operator, Meta-heuristic global optimization method, Swarm intelligence, Particle swarm optimization

1 Introduction

Energy production from fossil fuels accounts for over global greenhouse gas emissions of 75% and carbon dioxide emissions of 90% [1–3]. The ensuing global climate change further affects the production efficiency of renewable energy. Therefore, it is imperative to rapidly develop renewable energy as an alternative to achieve global decarbonization. Wind energy contributes 25.16% to electricity production among the various renewable energy sources, ranking second only to hydropower at 44.44% [4]. However, renewable energy itself

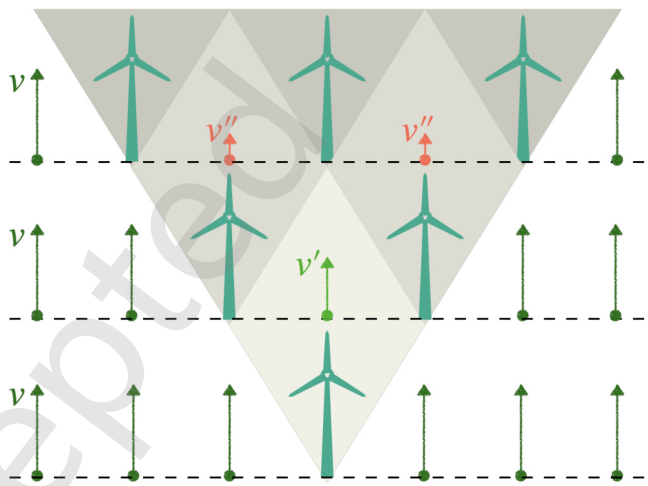

Fig. 1 Wake effect illustration.

also has significant environmental impacts [4–6]. Although wind farms can cause adverse ecological impacts such as land erosion, deforestation, visual disturbance, and noise [7], wind turbines have the least environmental impact among various renewable energies, whereas hydropower has the most significant impact and needs to be further replaced in the future [1]. Thus, as a low-impact, emission-free, green, and sustainable energy source, wind farms are highly suitable for large-scale development and implementation to combat the ecological and economic impacts of climate change. Between 2010 and 2021, the costs of offshore and onshore wind power decreased by 60% and 68%, respectively [1], and have been widely utilized [8], demonstrating the economic and application potential of wind energy on the path to decarbonization. Meanwhile, recent manufacturing, control, and optimization technologies have made wind turbines efficient, reliable, and durable [9].

An important and challenging problem in wind farms is the WFLOP. Due to the wake effect as shown in Fig. 1, upstream turbines of the wind farm absorb wind kinetic energy, causing downstream turbines, especially those located close by, to be affected by turbulence and therefore lack sufficient wind energy input for energy conversion. This phenomenon leads to so-called wake-effect losses, which refer to the reduction in power output of downstream turbines caused by energy

• Tao Zheng, Wenzhu Gu, Zhenyu Lei, and Shangce Gao are with the Faculty of Engineering, University of Toyama, Toyama-shi 930-8555, Japan. E-mail:113114zt@gmail.com, gushcerriy@outlook.com, leizg@eng.u-toyama.ac.jp, gaosc@eng.u-toyama.ac.jp(✉)
• Sichen Tao is with the Cyberscience Center, Tohoku University, Japan. E-mail: sichen.tao@tohoku.ac.jp
Manuscript received: 2026-1-16; revised: 2026-3-3; accepted: 2026-6-4

deficits and increased flow turbulence generated by upstream turbines. When turbines cannot fully utilize their rated energy conversion power, the overall energy conversion efficiency of the wind farm decreases. Therefore, optimizing the placement of turbines within a wind farm is directly related to the efficiency of wind energy utilization. Using more suitable and advanced methods to optimize the layout of turbines in a wind farm can enhance the overall energy conversion efficiency or make single optimization results more stable [10, 11]. Each percentage point increase in efficiency could bring millions to tens of millions of dollars in profit to a wind farm [12, 13], making WFLOP worthy of further exploration and resolution [14].

According to the wake model constructed by Jensen [15], Mosetti et al. firstly formulated and introduced WFLOP [16], and designed a genetic algorithm to solve it. Subsequently, Grady et al. obtained better solutions by increasing the number of initialized individuals and 3000 iterations [17]. Due to the limitations of traditional mathematical methods, such as excessive computational demands and the tendency to get trapped in local optima, new mathematical programming algorithms have been proposed, such as mixed integer programming [18], convex programming [19], etc. Additionally, due to their ease of use and excellent global search performance, metaheuristic algorithms have also been used to design and solve WFLOP, such as simulated annealing algorithm [20], ant colony optimization approach [21], global optimization strategy [22], Coral Reef algorithm [23], and random search algorithm [24]. Recent studies have extensively investigated optimization strategies for WFLOP from both algorithmic and application perspectives. Existing research can generally be categorized into mathematical programming methods, evolutionary algorithms, and swarm intelligence approaches. Mathematical programming techniques provide theoretical guarantees but often suffer from scalability limitations in large and constrained wind farm scenarios. Evolutionary algorithms, particularly genetic algorithm variants, have demonstrated strong robustness and flexibility under diverse wind conditions [25]. Meanwhile, swarm intelligence methods have attracted increasing attention due to their efficient population-based search mechanisms and competitive performance in complex optimization landscapes [26]. Recent survey and comparative studies indicate that balancing exploration and exploitation while effectively utilizing population information remains a central challenge in WFLOP optimization. These observations highlight the necessity of developing more adaptive search mechanisms tailored to WFLOP characteristics [27, 28].

In recent years, genetic algorithms (GA) have been widely used to solve WFLOP due to their excellent applicability and ease of use. Chen and MacDonald proposed a GA optimizer that considered some additional constraints in WFLOP [29]. Chen et al. proposed a GA to optimize the 2D wind farm layout for wind turbines of different heights [30]. Gao et al. proposed a multi-population GA to study 2D WFLOP incorporating the Jensen-Gaussian wake model [31]. Yin et al. developed a binary GA integrated with a binary submatrix to help combat production risks under wind uncertainty and conducted experiments in a simulated risk management model [32]. Parada et al. used a classical GA to optimize WFLOP based on the Gaussian wake model [33]. Recently, inspired and influenced by natural phenomena, two high-performance GAs have been proposed to solve WFLOP. First, in nature, the process of natural selection is influenced not only by gene control but also by the self-adjustment capabilities of individuals [34, 35]. Ju et al. applied this idea to GA and proposed an adaptive GA (AGA) and a self-informing genetic algorithm (SIGA) with Monte Carlo simulation based MARS regression [13]. The newly incorporated information exchange strategy inspired by natural phenomena significantly improved GA performance in WFLOP. Furthermore, a new self-informing genetic algorithm guided by support vector regression, called SUGGA, was proposed, which exhibited much better performance [14]. SUGGA utilizes support vector machine sampling and provides a more efficient surrogate model, thus more accurately guiding GA in search and optimization behaviors that align with WFLOP characteristics.

Despite different assumptions in WFLOP, such as varying wind turbine heights and land shapes, the core task is to find an effective algorithm to determine the optimal wind turbine layout. To this end, since obtaining source code from previous WFLOP studies is scarcely available for researchers [14], Ju et al. developed and provided an open-source Python package. This offers a benchmark research and testing platform for WFLOP (including a traditional GA and three advanced GAs: AGA, SIGA, and SUGGA, which can be used as benchmark algorithms), making related research convenient, reproducible, and comparable. Based on this, researchers can easily test, apply, research, and develop WFLOP itself and focus on exploring new methods. Moreover, this Python toolbox allows researchers to set wind farm size, wind speed profiles, wind turbine characteristics, and the number of wind turbines, and includes visualization functions and the MARS approximation algorithm. Therefore, leveraging the existing platform to further test and enhance WFLOP optimization algorithm performance is now feasible [36]. Recently, an intelligent metaheuristic algorithm based on the PSO search paradigm, a new particle swarm optimization with worst turbine replacement mechanism (AGPSO), was proposed and comprehensively compared with the benchmark algorithms integrated into the benchmark research and testing library established by Ju et al. [37]. Statistical results show that AGPSO exhibits significantly better optimization performance under various wind conditions and constraints compared to the previously verified best-performing SUGGA. Although genetic algorithm-based approaches have demonstrated strong applicability and flexibility in solving WFLOP, their performance often depends heavily on problem-specific operators and surrogate modeling strategies. Many GA variants improve solution quality through enhanced sampling or information exchange mechanisms; however, they may suffer from slow convergence and limited exploitation efficiency when the solution space structure becomes relatively regular [38]. These limitations suggest that alternative search paradigms with stronger directional guidance mechanisms may further improve optimization efficiency for WFLOP [39–41]. Against the backdrop of the widespread use of GA in solving WFLOP, this inspires us to consider and focus on the positive impact and unique effectiveness of the PSO evolutionary paradigm in addressing WFLOP. Although AGPSO has improved the performance of GLPSO [42] with a strategy based on WFLOP problem characteristics, its core optimization technique remains GLPSO. GLPSO was initially designed and proposed in 2015 to solve certain theoretical benchmark test sets with complex solution spaces. For theoretical universality, it adopted relatively conservative particle guiding vectors [43]. This likely leads to underutilization of computational resources when solving WFLOP, which has a relatively simple solution space, thus failing to generate diverse solutions while maintaining performance. Despite these advances, existing WFLOP optimizers still exhibit several structural limitations that restrict their adaptability and search efficiency, motivating further redesign of the underlying optimization mechanism. Moreover, according to no-free-lunch theorem [44], redesigning and adjusting an optimizer specifically for a new problem can bring significant performance gains. Building upon the above observations, several structural limitations can be summarized as follows. First, in GLPSO and AGPSO, particle guidance mainly relies on fixed hierarchical relationships and limited guiding vectors, which were originally designed for general benchmark problems rather than WFLOP [45]. As a result, high-quality layout information cannot be sufficiently exploited, leading to inefficient utilization of elite individuals. Second, WFLOP is characterized by a structured and constrained search space, where candidate solutions often exhibit clear performance stratification. However, existing PSO-based methods treat particles with different solution qualities in a largely uniform manner, which weakens the balance between elite exploitation and population diversity maintenance. Third, current PSO-based WFLOP algorithms lack explicit mechanisms to coordinate multi-layer population information and multi-directional learning, limiting their adaptability in complex and highly constrained scenarios. Motivated by these identified limitations, this study redesigns the core guidance mechanism of PSO from a hierarchical and directional perspective, explicitly addressing inefficient elite utilization, insufficient multi-layer information interaction, and limited directional learning capability in existing WFLOP optimizers. By explicitly constructing multiple guidance directions among particles with different quality levels, a more flexible and problem-oriented search paradigm can be established [46]. This forms the fundamental motivation for developing the proposed level-direction guided hierarchical particle swarm optimization (HGPSO), which enhances information utilization efficiency and search balance in WFLOP.

These observations motivate the introduction of hierarchical population organization and directional learning mechanisms. To further explore and leverage the potential and performance of the PSO paradigm in solving WFLOP, we propose a hierarchical PSO using elite level-direction to enhance the performance of existing state-of-the-art WFLOP PSO. Combined with the adaptive replacement strategy from AGPSO, we develop and propose a level-direction guided hierarchical particle swarm optimization based on GLPSO and AGPSO, called HGPSO, to further enhance PSO's performance in solving WFLOP from the core optimization technique level [47]. HGPSO utilizes the three naturally existing hierarchical individuals in GLPSO to construct novel optimization operators based on four different guiding vectors, replacing the core optimization operators in GLPSO and AGPSO. The new HGPSO search paradigm can better align PSO's search behavior with WFLOP characteristics under a fixed evaluation budget. The proposed method maintains solution diversity during exploration. Meanwhile, it converges rapidly toward high-quality regions of the search space. As a result, robust and reliable solutions are obtained. Additionally, the newly proposed PSO operators correct and avoid the substantial repetitive searches caused by encoding problems when introducing PSO operators in AGPSO, thereby reducing redundant evaluations caused by encoding-related invalid updates. Unlike existing PSO variants and hybrid metaheuristics that mainly improve WFLOP performance through problem-specific heuristics or external operators, HGPSO fundamentally redesigns the core PSO update mechanism by introducing a level-direction guided hierarchical search framework. This framework enables multi-layer information interaction and multi-directional guidance within the population, thereby achieving more effective exploration–exploitation balance for WFLOP.

To verify the effectiveness and efficiency of HGPSO, we conducted extensive testing and validation under 156 different combinations involving 4 wind conditions, 3 turbine layout quantities, and 13 land use conditions considering landowner participation behavior (including 12 restricted conditions). In all tests, for comparison purposes, we used five state-of-the-art metaheuristic algorithms from recent WFLOP studies and three state-of-the-art metaheuristic algorithms in theoretical tests, covering four types of classic search paradigms. The experimental results indicate that HGPSO achieves consistently competitive performance across diverse WFLOP settings. Besides, HGPSO also has some other features. Compared with AGPSO, which improves WFLOP performance mainly through application-oriented strategies, the proposed HGPSO focuses on enhancing the intrinsic PSO search dynamics. Therefore, the contribution of this work lies not only in performance improvement but also in introducing a new hierarchical learning paradigm for PSO-based WFLOP optimization.

The main contributions and originality of this paper are summarized as follows:

1) We propose a novel level-direction hierarchical particle swarm optimization (HGPSO), which is based on the first diversified and hierarchical improvements of core PSO optimization techniques on WFLOP. This represents the first systematic attempt to integrate hierarchical learning and directional guidance into PSO for WFLOP. The source code of HGPSO will be open-sourced in response to Ju et al.'s call for establishing a WFLOP benchmark platform and benchmark algorithm library [13, 14], enriching the library with a new efficient PSO algorithm as well as providing reproducibility. This will further facilitate researchers in reproducing, testing, and developing new high-performance WFLOP methods, effectively accelerating related research progress.
2) Extensive experiments under diverse wind conditions, turbine budgets, and land-use constraints verify that HGPSO can provide competitive layouts. These layouts offer multiple feasible options for decision-making under land negotiation and procurement considerations. Based on this, wind power companies can proactively make flexible economic decisions because diverse land use and wind farm layout options can effectively reduce the costs of negotiating for wind farm land and purchasing turbines while improving the overall energy conversion efficiency of turbines and related economic benefits.
3) This article provides comprehensive comparative results for six state-of-the-art WFLOP optimizers and three advanced metaheuristic methods. These results offer valuable references for future research and practical applications. Additionally, representative layout visualizations show that HGPSO can generate feasible layouts with relatively organized spatial patterns in several constrained WFLOP scenarios. This observation is used as supplementary visual evidence, while the main performance conclusions are supported by conversion efficiency, convergence behavior, solution distributions, and statistical tests.

The rest of this paper is as follows: Section 2 introduces WFLOP, including the related equations, the wake model, the power curve, and the objective function; Section 3 presents the HGPSO algorithm; Section 4 validates the proposed HGPSO algorithm and other advanced WFLOP benchmark algorithms, as well as advanced metaheuristic algorithms, through a series of numerical experiments under different types of wind farm scenarios; Section 5 discusses the findings and concludes the paper.

2 The wind farm layout optimization problem

The Wind Farm Layout Optimization Problem (WFLOP) aims to determine the optimal spatial positions of wind turbines within a given wind farm area in order to maximize energy production while satisfying practical constraints. In this section, we present the objective function, wake model, and power curve model from the wind farm optimization benchmark testing platform recently established by Ju et al., which considers the total construction cost and power generation of the wind farm.

2.1 Optimization objective

The objective of WFLOP is to arrange turbine positions within the wind farm so as to reduce wake-induced power losses and improve the overall power generation performance under the given turbine and land resources. More explicitly, the WFLOP considered in this paper is a constrained layout optimization problem. The decision variable is the turbine layout L, which determines the grid locations and the corresponding physical coordinates of all turbines in the wind farm. The optimization objective is to maximize the expected total power generation of the wind farm under the given wind-speed and wind-direction distribution. Since the number of turbines is fixed in each test instance, maximizing the cost-normalized power generation in Eq. (1) is equivalent to maximizing the total generated power in Eq. (3). The total power is further calculated by Eq. (4), where wake-induced wind-speed deficits are evaluated using the wake model introduced in Section 2.2 and turbine power is obtained from the power curve in Eq. (12). The main constraints of the WFLOP include wind-farm boundary constraints, land-use restricted-area constraints, duplicate-location constraints, and minimum inter-turbine spacing constraints. In the adopted benchmark setting, these constraints are handled through the grid-based encoding and boundary detection mechanisms described in Sections 3.1.2 and 3.3. Specifically, turbine locations must be selected from feasible grid cells within the wind-farm boundary, cannot be placed in restricted areas, and cannot overlap with other turbines. In addition, the grid-cell width is set to 231 m, which equals three rotor diameters of the adopted turbine, so distinct grid indices automatically satisfy the minimum inter-turbine spacing requirement. Therefore, the optimization problem is evaluated by the objective function in Section 2.1 while feasibility is maintained through the constraint-handling mechanism described later in the algorithmic procedure. The mathematical expression is as follows:

$$Maximize\ \ f(x) = \frac{P_{total}(N, L)}{C_{total}(N)} \tag{1}$$

where, N represents the number of turbines installed in a wind farm. L represents the turbine layout in the wind farm. $P_{total}(N, L)$ represents the wind farm total power generation with N turbines in layout L. $C_{total}(N)$ represents the cost of constructing the wind farm with N turbines. The cost formula for the wind farm $C(N)$ is expressed as follows:

$$C_{total}(N) = N \cdot (\frac{2}{3} + \frac{1}{3} \cdot e^{-0.00174 \cdot N^2}) \tag{2}$$

where, when N is very large, the turbine cost tends towards $\frac{2}{3} \cdot N$. When the turbine number is fixed, the cost is a constant value. Therefore, for a given turbine problem, the objective function can be simplified as follows:

$$Maximize\ \ f(x) = P_{total}(L) \tag{3}$$

where, the specific layout L directly influences and determines the total power P_{total} of the wind farm, which is determined by wind speed, wind direction, layout, and the number of turbines, and is expressed as follows:

$$P_{total}(L) = \sum_{i=1}^{N} \sum_{\theta, V} p(\theta, V) \cdot P_i(\theta, V, L) \tag{4}$$

where, $p(\theta, V)$ represents the probability distribution of wind direction and wind speed. The definition of wind direction on coordinates is shown in Fig. 2. $P_i(\theta, V, L)$ represents the power of the i-th turbine placed in the wind farm with layout L under wind direction θ and wind speed V. As a decision variable, L directly influences the power output of each turbine, thereby determining the total power of the wind farm. To facilitate quantification and ease of reference, the conversion efficiency η is introduced to measure the effectiveness of the wind farm layout, expressed as follows:

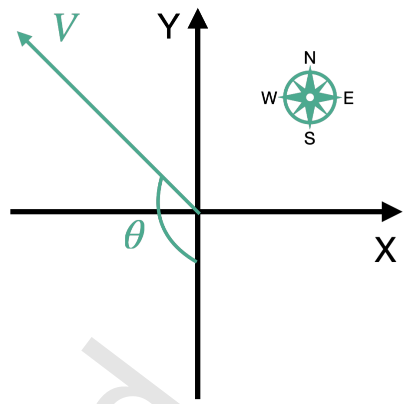

Fig. 2 Definition of wind speed direction based on coordinates.

$$\eta = \frac{P_{total}(N, L)}{N \cdot \sum_{\theta, V} p(\theta, V) \cdot P_{rate}(V)} \tag{5}$$

where, as a criterion for evaluating the effectiveness of different turbine layouts in a wind farm to mitigate wake effects, η is expressed as the ratio of actual output power to ideal output power. It intuitively represents the energy utilization efficiency within the wind farm.

2.2 Jensen wake model

In this paper, the classical Jensen wake model is adopted to evaluate wake-induced wind-speed deficits among turbines [48]. This model has been widely used in WFLOP studies because of its simple structure, low computational cost, and good compatibility with population-based layout optimization algorithms. In the adopted benchmark framework, the Jensen wake model is used to determine the wake expansion radius and the effective wind speed received by downstream turbines under each wind direction and wind speed scenario. Under the assumption of momentum conservation [15, 49], the following formula can be derived:

$$\pi \cdot r_i^2 \cdot V' + \pi \cdot (R_{d_{i,j}}^2 - r_i^2) \cdot V = \pi \cdot R_{d_{i,j}}^2 \cdot v \tag{6}$$

where, V is the environment wind speed. V' is the wind speed after passing through a turbine, which is approximated as $1/3 \cdot V$ [49]. v is the wind speed affected by the wake effect from upstream turbines, which is used to calculate the power conversion of the downstream turbines. As shown in Fig. 3, r_i and $R_{d_{i,j}}$ are the radius of turbine i and the radius of

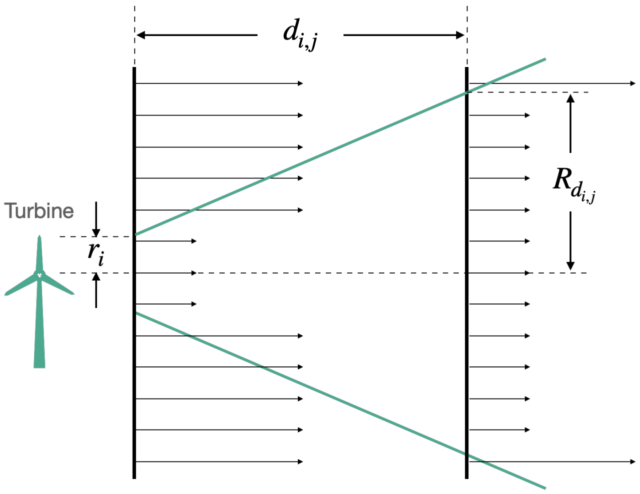

Fig. 3 Diagram of the wake effect model.

the wake effect at distance $d_{i,j}$ downwind from this turbine, respectively, affecting another turbine j. Based on Eq. (6), the expression for v is derived as follows:

$$v = [1 - \frac{2}{3} \cdot (\frac{r_i}{R_{d_{i,j}}})^2] \cdot V \tag{7}$$

where, the wake effect radius R_d produced by turbine i at a certain distance d is assumed to be related to the turbine radius r_i and is proportional to the distance d. Its formula is expressed as follows:

$$R_{d_{i,j}} = r_i + \alpha_i \cdot d_{i,j} \tag{8}$$

where, $d_{i,j}$ represents the distance between turbine j and turbine i. The value α_i of turbine i is considered to be related to the hub height of turbine i and the surface roughness of the wind farm, and its calculation formula is as follows:

$$\alpha_i = 0.5 \cdot (ln \frac{h_i}{z_0})^{-1} \tag{9}$$

where, h_i represents the hub height of turbine i. z_0 represents the surface roughness of the wind farm. On sandy ground, z_0 typically ranges between $[0.2, 0.3]$ (mm).

Due to the fact that any turbine may frequently be affected by the combined wake effects of multiple upstream turbines [49], the following equation is derived:

$$(1 - \frac{v_j}{V})^2 = \sum_{i \in \Phi_j} (1 - \frac{v_{i,j}}{V})^2 \tag{10}$$

where, Φ_j represents the set of indices of all turbines upstream of turbine j that cause wake effects on turbine j. $v_{i,j}$ represents the input wind speed to turbine i considering only the wake effect caused by turbine j. Solving Eq. (10) yields the following:

$$v_j = V \cdot [1 - \sqrt{\sum_{i \in \Phi_j} (1 - \frac{v_{i,j}}{V})^2}] \tag{11}$$

where, v_j is the input wind speed at turbine j after considering the wake effects from all upstream turbines. The power P_j of the turbine can be easily calculated based on the power curve as follows [49]:

$$P_j = P(v_j) = \begin{cases} 0 & , \text{if } v_j < 2 \\ 0.3v_j^3 & , \text{if } 2 \leqslant v_j < 12.8 \\ 629.1 & , \text{if } 12.8 \leqslant v_j \leqslant 18 \\ 0 & , \text{if } v_j > 18 \end{cases} \tag{12}$$

where, the unit of power is kW. The unit of wind speed is m/s. The power curve is shown in Fig. 4. Therefore, throughout this study, all objective-function evaluations are based on the Jensen wake model. This setting ensures that HGPSO and the compared WFLOP benchmark algorithms are evaluated under the same aerodynamic model, making the optimization results comparable.

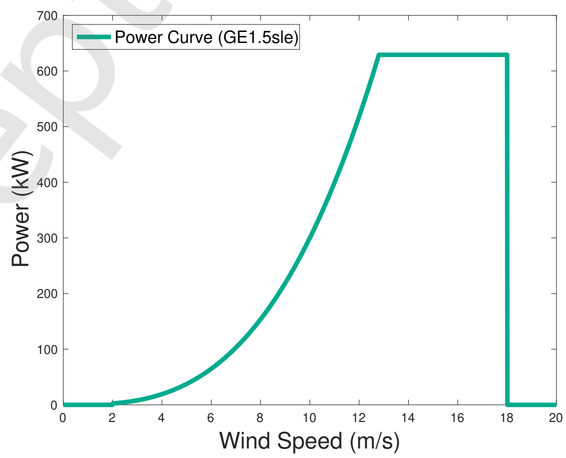

Fig. 4 The plot of the GE1.5sle power curve.

3 A novel PSO variant for WFLOP

In this section, we first introduce AGPSO, which has demonstrated strong performance in the WFLOP benchmark library [37], and then present the proposed level-direction guided hierarchical particle swarm optimization (HGPSO). For readability, Section 3 is organized into smaller components, namely initialization and encoding, exemplar construction, constraint handling, hierarchical update rules, and algorithmic workflow. Before introducing the optimization procedures, it is worth noting that the fitness of each candidate layout is determined directly by the wind-energy conversion model in Section 2. In particular, turbine power is computed from the power curve shown in Fig. 4, which maps the effective wind speed at each turbine to its generated power. Therefore, the optimization process of HGPSO is guided by physically meaningful energy conversion characteristics rather than by an abstract synthetic objective.

Table 1 Main symbols used in AGPSO and HGPSO.

Symbol	Meaning	Symbol	Meaning
NP	population size	D	decision dimension; under the adopted index encoding, $D = N$
N	number of turbines	I_r, I_c	numbers of grid rows and columns
$x_i^{(k)}$	current particle/layout of individual i at iteration k	$x_{i,j}^{(k)}$	j-th decision variable of $x_i^{(k)}$
$e_i^{(k)}$	reference individual after crossover, mutation, and selection	$x_g^{(k)}$	global best individual
$v_i^{(k)}$	velocity/update increment of particle i	c	acceleration coefficient in the PSO update
p_m	mutation probability	s	stagnation threshold before tournament replacement
m	branch threshold controlling the directional preference in HGPSO	W_t	grid-cell width used to map indices to physical coordinates
WF	feasible grid-index set of the wind farm	CL	all land-use restricted grid indices
$E(\cdot)$	encoding operator from a feasible index solution to physical turbine coordinates	$R(\theta)$	rotation matrix for wake evaluation at wind direction θ
tr	replacement candidate drawn from the high-quality cumulative-power pool	$maxFEs$	maximum number of function evaluations

3.1 Adaptive PSO with worst replacement mechanism

3.1.1 Population initialization and exemplar update

In AGPSO, the initial population stores NP individuals, each representing a WFLOP solution. The population is gradually optimized through evolutionary iterations to obtain better solutions. The population is represented as follows:

$$P_x^{(k)} = \{x_1^{(k)}, x_2^{(k)}, ..., x_i^{(k)}, ..., x_N^{(k)}\} \tag{13}$$

where, $x_i^{(k)}$ represents the i-th individual in the k-th generation population. $P_x^{(k)}$ represents the population of the k-th generation. Each individual in the population is represented as follows:

$$x_i^{(k)} = \{x_{i1}^{(k)}, x_{i2}^{(k)}, ..., x_{ij}^{(k)}, ..., x_{iD}^{(k)}\} \tag{14}$$

where, $x_{ij}^{(k)}$ represents the solution value of the j-th dimension in the i-th individual from the k-th iteration population. Under the adopted index encoding, each dimension stores one turbine-location index and therefore $D = N$, namely the number of turbines. If one directly optimized 2D physical coordinates, the dimension would be $2N$; however, that is not the representation used in AGPSO or HGPSO.

In each iteration, AGPSO performs a series of identical calculations to gradually optimize the population quality and obtain better WFLOP solutions. First, based on the information in each dimension j of the best individual $x_g^{(k)}$ in the population, a crossover operator is implemented as follows:

$$e_{i,j}^{(k)} = \begin{cases} rand_1(0,1) \cdot x_{i,j}^{(k)} + (1 - rand_2(0,1)) \cdot x_{g,j}^{(k)}, \\ \qquad \text{if } f(x_i) > f(x_{rand}), \\ x_{rand,j}^{(k)}, \text{otherwise.} \end{cases} \tag{15}$$

where, $rand_1$ and $rand_2$ denote two independent random numbers uniformly distributed in [0,1]. $x_{rand,j}^{(k)}$ represents the value of the j-th dimension of a random individual in the k-th generation population, used to replace individuals that failed to update. $f(x_i)$ represents the evaluation value obtained by x_i in the evaluation function, i.e., $\eta_{x_i} = f(x_i)$. $rand(0,1)$ denotes a random number between [0, 1]. e represents a newly updated individual (solution). Thereafter, based on a threshold probability p_m and the upper and lower boundaries of each dimension in the solution space, a basic mutation strategy is implemented to further update this new individual e. The process is expressed as follows:

$$e_{i,j}^{(k)} = rand(lb_j, ub_j), \text{ if } rand(0,1) < p_m \tag{16}$$

where, $rand(lb_j, ub_j)$ and $rand(0,1)$ represent random numbers within the ranges $[lb_j, ub_j]$ and $[0,1]$, respectively. In the index-encoding setting, $[lb_j, ub_j] = [1, I_r I_c]$, so the mutation operator always samples inside the global wind-farm grid bounds before the subsequent discrete feasibility repair. lb_j and ub_j denote the lower and upper boundaries of any individual x in dimension j. Then, an evaluation is performed using the objective function to implement an elite selection mechanism, expressed as follows:

$$e_{i,j}^{(k)} = \begin{cases} e_{i,j}^{(k)} & \text{, if } f(e_i^{(k)}) > f(x_i^{(k)}) \\ x_{i,j}^{(k)} & \text{, otherwise} \end{cases} \tag{17}$$

where, since $e_{i,j}^{(k)}$ is an important leverage variable, it will provide crucial information in the subsequent core operations of PSO. Therefore, a counter is also introduced here. If an individual at the same index position in X fails to obtain a better solution after being updated s times cumulatively, then $e_{i,j}^{(k)}$ is further optimized through a tournament selection mechanism. Importantly, this tournament mechanism is activated only after s unsuccessful updates, which makes the replacement adaptive rather than unconditional. The tournament selects the best individual from 20% of randomly chosen individuals in the population to replace $e_{i,j}^{(k)}$, ensuring that the quality of $e_{i,j}^{(k)}$ does not degrade excessively. This fixed 20% tournament subset is distinct from the later worst-position replacement rule, whose candidate-pool size is adaptive. Finally, by updating a velocity variable $v_i^{(k)}$, $x_i^{(k)}$ is updated to obtain a new candidate solution, expressed as follows:

$$v_{i,j}^{(k)} = c \cdot rand(0,1) \cdot (e_{i,j}^{(k)} - x_{i,j}^{(k)}) \tag{18}$$

$$x_{i,j}^{(k+1)} = x_{i,j}^{(k)} + v_{i,j}^{(k)} \tag{19}$$

where, c is a speed parameter and $rand(0,1)$ represents a random number in the range $[0,1]$. The velocity and position updates in Eqs. (15)–(19) are performed iteratively at each generation. The velocity term is recalculated at every iteration based on the current reference individual and does not accumulate across generations. This design stabilizes convergence while maintaining adaptive search capability throughout the optimization process.

3.1.2 Boundary handling and worst-position replacement

Finally, a boundary detection and feasibility repair mechanism is implemented to enforce the spatial constraints of WFLOP. After each position update, all turbine indices in the newly generated layout are checked before fitness evaluation. A turbine position is regarded as infeasible if the selected index is outside the wind-farm boundary, duplicated with another turbine in the same layout, or belongs to the land-use restricted set CL. Once an infeasible turbine position is detected, the corresponding index is regenerated from the wind-farm grid domain. The expression for this feasibility repair process is given as follows:

$$\begin{aligned} x_{i,j}^{(k+1)} &= randi(1, I_r \cdot I_c), \\ &\text{if } (x_{i,j}^{(k+1)} \notin WF) \vee (x_{i,j}^{(k+1)} = x_{i,a}^{(k+1)}) \vee (x_{i,j}^{(k+1)} \in CL). \end{aligned} \tag{20}$$

where, I_r and I_c represent the maximum numbers of turbine positions that can be placed in rows and columns, respectively. $randi(1, I_r \cdot I_c)$ is a randomly generated integer between $[1, I_r \cdot I_c]$. WF is the feasible set of grid indices, namely $WF = \{1, 2, ..., (I_r \cdot I_c)\}$, and $x_{i,a}^{(k+1)}$ represents the $(k+1)$-th solution value for the a-th turbine in the i-th individual with $a \neq j$. CL denotes the complete set of land-use restricted indices where placing turbines is prohibited. In the implementation, the resampling implied by Eq. (20) is repeated until an admissible index is obtained, so the repaired solution always returns to the feasible discrete domain before wake evaluation. In the implementation, the boundary detection mechanism is applied before the worst-position replacement strategy. The former guarantees spatial feasibility, whereas the latter further improves the repaired layout by replacing the turbine position with the lowest cumulative power contribution.

To improve reader comprehension, Fig. 9 provides a visual illustration of the boundary detection mechanism associated with Eq. (20). The grid domain shown in Fig. 9 represents the allowable wind-farm bounds, while the shaded regions denote restricted areas where turbine placement is prohibited due to land-use constraints. During optimization, infeasible solutions may occur when turbine indices exceed the WF bounds, when turbines are located within CL, or when multiple turbines are assigned to the same grid position. In such cases, a new feasible turbine position is regenerated according to Eq. (20). The corresponding pseudocode in Algorithm 1 explicitly annotates boundary checking and worst-position replacement so that the full WFLOP-specific repair process can be followed directly.

Compact repair logic. *Step 1:* after every coordinate update, check whether the index lies outside WF, falls in CL, or duplicates another turbine index in the same layout. *Step 2:* if any of these violations occurs, repeatedly resample a new grid index from $[1, I_r I_c]$ until a feasible index is obtained. *Step 3:* once the whole layout is feasible, compute cumulative turbine-power statistics and identify the lowest-power position. *Step 4:* replace only that worst position with a candidate drawn from the high-quality cumulative-power pool $\Pi_i(1{:}K)$, which biases the repair toward informative regions without abandoning feasibility.

At the end of each iteration, the cumulative power generation for each turbine position in the wind field from the beginning of the iteration to the current point is accumulated. Based on this information, the turbine position with the lowest cumulative power generation in each solution is replaced by a new candidate drawn from a high-quality cumulative-power pool. The process is expressed as follows:

$$x_{i,w}^{(k+1)} = x_{i,tr}^{(k+1)}, \qquad tr \in \Pi_i(1:K), \qquad K = \lfloor r_w I_r I_c \rfloor + D \tag{21}$$

where, $x_{i,w}^{(k+1)}$ represents the index of the turbine position w with the lowest cumulative power generation in the i-th current solution, Π_i denotes the descending ranking of cumulative grid-power scores, and r_w is the base ratio controlling the size of the high-quality candidate pool. In the original implementation, $r_w = 0.1$. Hence, on the 12×12 benchmark grid, K becomes 29, 34, and 39 for $N = 15$, 20, and 25, respectively, corresponding to an effective candidate pool of approximately 20.1%, 23.6%, and 27.1% of the grid. This design prevents the replacement step from becoming overly greedy, helps avoid premature convergence, and maintains population diversity by reusing informative turbine positions without collapsing the search to only a few elite cells. Since the replacement pool is driven by cumulative turbine-power statistics rather than by a hand-crafted deterministic rule, the search is adaptively biased toward high-energy regions while remaining data-driven.

3.2 Level-direction guided hierarchical particle swarm optimization

3.2.1 *Mechanism-level motivation*

Despite the use of GLPSO [42] in AGPSO [37] revealing the suitability of PSO-type optimizers for WFLOP, AGPSO mainly improves performance through cumulative turbine-power information and worst-position replacement. Such enhancement is valuable, but it remains at the application level and does not explicitly redesign the underlying PSO learning rule itself. In contrast, HGPSO directly modifies the internal particle-learning behavior. This distinction marks a transition from application-level enhancement to mechanism-level PSO adaptation for WFLOP. The rationale for introducing hierarchical learning is that particles with different solution qualities should play different roles during the search process. Conventional PSO variants usually rely on a single global or neighborhood best solution, which may cause rapid information concentration and premature convergence. In contrast, HGPSO constructs a quality-based hierarchy using the current particle x_i, the reference particle e_i, and the global best particle x_g. The current particle mainly maintains exploration diversity, the reference particle provides intermediate guidance, and the global best particle supplies elite exploitation information. Through this structure, useful search information can be transferred progressively across different particle levels rather than only through direct global-best guidance, thereby improving information flow and balancing exploration and exploitation.

It should also be emphasized that the proposed HGPSO is different from conventional hierarchical PSO and multi-swarm PSO variants. Typical hierarchical PSO methods usually define a leader–follower topology or organize particles into predefined hierarchical layers, whereas multi-swarm PSO methods divide the population into several sub-swarms and coordinate their search through information exchange or migration. In contrast, HGPSO does not introduce additional sub-swarms, migration operations, or a fixed population topology. Its hierarchical characteristic is embedded in the update mechanism itself. Specifically, each particle update simultaneously considers the current particle x_i, the reference individual e_i, and the global best individual x_g, which represent different guidance levels in the search process. In this mechanism, x_g supplies elite guidance for exploiting high-quality search regions, while e_i serves as an intermediate guidance source that helps preserve directional diversity and reduce over-reliance on a single leader. Based on the hierarchical relationship among these individuals, HGPSO adaptively selects the corresponding update tendency through the case-based rules in Eqs. (22a)–(22f). Therefore, the novelty of HGPSO lies in the mechanism-level redesign of the PSO update rule for WFLOP, where elite guidance and directional diversity are jointly considered, rather than in simply adopting an existing hierarchical or multi-swarm population structure.

3.2.2 *Hierarchical update cases and design rationale*

To further investigate the applicability and performance potential of advanced PSO for WFLOP, this study proposes a new PSO operator that directly enhances the search mechanism itself. In HGPSO, the search process integrates both multi-direction and level-direction strategies. The multi-direction mechanism constructs candidate guiding directions from three representative individuals, namely the current particle x_i, the reference individual e_i, and the global best particle x_g. The level-direction mechanism then regulates which direction becomes dominant according to the hierarchical relationship among these three individuals. Consequently, HGPSO can maintain population diversity while steadily improving overall solution quality under the same evaluation budget.

More specifically, "level-direction guidance" consists of two components. The "level" component denotes the hierarchical relationship among x_i, e_i, and x_g, where x_i is the current particle, e_i is the reference individual generated through evolutionary operations, and x_g is the global best individual. The "direction" component denotes the update tendency determined by this hierarchical relationship rather than a single fixed vector. In HGPSO, the main update tendencies include reference-guided update, global-best-guided update, and elite-relay-guided update. These tendencies are incorporated into the particle update through the case-based rules in Eqs. (22a)–(22f), where each case corresponds to a specific relationship among x_i, e_i, and x_g. Therefore, level-direction guidance provides a mechanism-level redesign of the PSO update rule by adaptively selecting the guidance tendency during the search process.

Let m denote the branch threshold controlling the directional preference in HGPSO. In the original implementation,

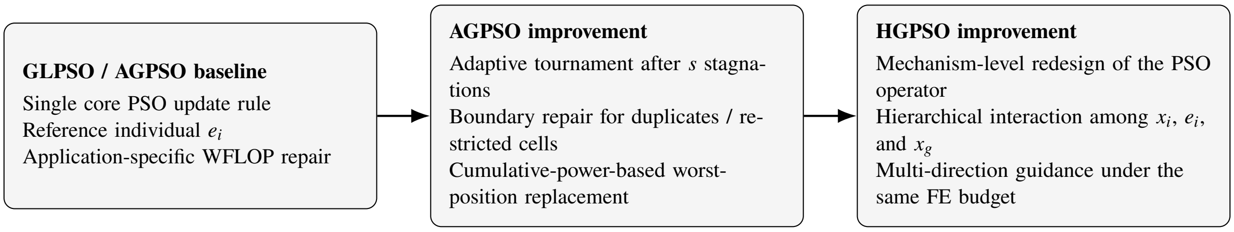

Fig. 5 Evolution from AGPSO to HGPSO: AGPSO mainly adds WFLOP-specific repair, whereas HGPSO further redesigns the PSO search operator.

$m = 0.9$, meaning that the second branch is selected with high probability and therefore gives stronger preference to the elite-relay direction when the current particle, the reference individual, and the global best solution are all different. Unlike the mutation probability p_m in Eq. (16), which introduces random perturbations, m regulates how search effort is distributed between alternative guiding directions inside the PSO operator itself.

Using sub-equation numbering, the HGPSO update rule can be written as follows:

$$x_{i,j}^{(k+1)} = lb_j + (ub_j - lb_j) \cdot rand(0,1), \quad \text{if } x_{i,j}^{(k)} = e_{i,j}^{(k)},\ x_{i,j}^{(k)} = x_{g,j}^{(k)}, \tag{22a}$$

$$x_{i,j}^{(k+1)} = x_{i,j}^{(k)} + c \cdot rand(0,1) \cdot \left(x_{g,j}^{(k)} - x_{i,j}^{(k)}\right), \quad \text{if } rand(0,1) < 1-m,\ x_{i,j}^{(k)} = e_{i,j}^{(k)},\ x_{i,j}^{(k)} \neq x_{g,j}^{(k)}, \tag{22b}$$

$$x_{i,j}^{(k+1)} = x_{i,j}^{(k)} + c \cdot rand(0,1) \cdot \left(e_{i,j}^{(k)} - x_{i,j}^{(k)}\right), \quad \text{if } rand(0,1) < 1-m,\ x_{i,j}^{(k)} \neq e_{i,j}^{(k)}, \tag{22c}$$

$$x_{i,j}^{(k+1)} = x_{i,j}^{(k)} + c \cdot rand(0,1) \cdot \left(e_{i,j}^{(k)} - x_{i,j}^{(k)}\right), \quad \text{if } rand(0,1) \geqslant 1-m,\ x_{i,j}^{(k)} \neq e_{i,j}^{(k)},\ x_{i,j}^{(k)} = x_{g,j}^{(k)}, \tag{22d}$$

$$x_{i,j}^{(k+1)} = x_{i,j}^{(k)} + c \cdot rand(0,1) \cdot \left(x_{g,j}^{(k)} - x_{i,j}^{(k)}\right), \quad \text{if } rand(0,1) \geqslant 1-m,\ x_{i,j}^{(k)} = e_{i,j}^{(k)},\ x_{i,j}^{(k)} \neq x_{g,j}^{(k)}, \tag{22e}$$

$$x_{i,j}^{(k+1)} = e_{i,j}^{(k)} + c \cdot rand(0,1) \cdot \left(x_{g,j}^{(k)} - e_{i,j}^{(k)}\right), \quad \text{if } rand(0,1) \geqslant 1-m,\ x_{i,j}^{(k)} \neq e_{i,j}^{(k)},\ x_{i,j}^{(k)} \neq x_{g,j}^{(k)}. \tag{22f}$$

In Eqs. (22a)–(22f), $rand(0,1)$ denotes a random number uniformly generated in $[0,1]$, and ub_j and lb_j represent the upper and lower bounds of the j-th dimension in the current WFLOP. The six cases make the search logic easier to interpret. Case (22a) reinitializes a fully stagnant dimension. Cases (22b) and (22e) move the particle directly toward the global best solution when the reference individual does not provide additional directional novelty. Cases (22c) and (22d) exploit the reference direction. Finally, Case (22f) uses the relay direction from e_i to x_g, which is the key mechanism-level addition distinguishing HGPSO from a single-leader PSO. Therefore, when all three representatives disagree, HGPSO does not merely follow one leader; instead, it adaptively chooses whether to exploit the reference direction or the elite-relay direction, which improves the exploration–exploitation balance. The computational overhead of the proposed level-direction guided update is limited because Eq. (22) only introduces a constant number of conditional comparisons and arithmetic operations for each decision dimension. Therefore, the optimizer-side update cost remains comparable to that of PSO-family algorithms. The dominant computational cost in WFLOP still comes from wake-effect evaluation and power calculation. A detailed time and space complexity analysis is provided in Appendix A.2, where the total runtime and memory requirements of HGPSO are discussed.

Additionally, AGPSO may waste evaluations when $e_{i,j}^{(k)} = x_{i,j}^{(k)}$, because the induced update in Eqs. (18) and (19) becomes ineffective. The conditional structure in Eqs. (22a)–(22f) explicitly distinguishes these coincidence cases, thereby reducing invalid moves and improving the efficiency with which the fixed FE budget is used.

To further explain the observed efficiency improvement, it should be noted that all algorithms in this study are executed under an identical computational budget defined by the same maximum number of function evaluations. Therefore, improvements in optimization performance achieved within the same evaluation limit directly indicate more effective utilization of computational resources.

To provide an intuitive understanding of the multi-layer and hierarchical organization employed in HGPSO, Fig. 6 illustrates the population structure and the corresponding information interactions among different solution-quality levels. In the proposed framework, the hierarchy does not refer to algorithmic stages but to a quality-based organization of particles within the population. Specifically, each particle is associated with three representative individuals with progressively improved solution quality, namely the current particle x_i, the reference particle e_i, and the global best particle x_g. These individuals form three distinct layers: the individual layer, the intermediate guidance layer, and the elite layer. The individual layer (x_i) represents ordinary particles responsible for exploration of the search space. The intermediate layer (e_i) provides refined guidance generated through evolutionary interactions and serves as a bridge between exploration and exploitation. The elite layer (x_g) corresponds to the globally best solution and supplies global exploitation guidance. As illustrated in Fig. 6, hierarchical learning is realized through structured information propagation across layers as well as interactions within the same layer. Vertical information flow enables particles to learn from higher-quality individuals, while horizontal interactions help preserve diversity among particles of comparable quality. Through this multi-layer organization, HGPSO establishes a clear hierarchical learning structure that differs from conventional PSO variants relying primarily on single-level guidance. This figure therefore provides an intuitive visualization of how hierarchical relationships are defined and how multi-layer information interaction supports the level-direction guided search mechanism in HGPSO.

3.2.3 *Algorithmic workflow*

Algorithm 1 HGPSO

Input: Parameters D, NP, $maxFEs$, and $nFEs$.
Output: The optimized WFLOP solution.
Initialization: Generate a fresh population $P_x^{(1)}$ with NP agents and $D = N$ decision variables (one grid index per turbine).
Search phase:
Boundary detection of $x_i^{(1)}$ by Eq. (20) to remove out-of-bound, duplicate, and restricted-cell assignments;
Evaluate $\eta_{x_i^{(1)}} = f(x_i^{(1)})$ for every individual; set the iteration counter $k = 1$;
while $nFEs < maxFEs$ **do**
  for i = 1 to NP **do**
    Calculate the best individual $x_g^{(k)}$ in the current population;
    Op.1: Update the reference individual $e_i^{(k)}$ by Eq. (15);
    Op.2: Apply the basic mutation strategy to $e_i^{(k)}$ by Eq. (16);
    Op.3: Select between $e_i^{(k)}$ and $x_i^{(k)}$ by Eq. (17);
    Op.4: Generate the trial solution $x_i^{(k+1)}$ by Eq. (22) using $e_i^{(k)}$, $x_g^{(k)}$, and $x_i^{(k)}$;
    Boundary detection of $x_i^{(k+1)}$ by Eq. (20);
    Conduct the worst replacement strategy by Eq. (21);
    Evaluate the fitness value $f(x_i^{(k+1)})$ in the current population;
    Conduct the selection operator between $x_i^{(k)}$ and $x_i^{(k+1)}$ using Eq. (17);
  end for
  Record the current optimal solution $x_g^{(k+1)}$ and its fitness value $\eta_{x_g^{(k+1)}} = f(x_g^{(k+1)})$;
  Update the iteration number with $k = k + 1$;
  Update the evaluation number with $nFEs = nFEs + NP$;
end while
Output the optimal solution $x_{out} = x_g^{(k)}$ and the corresponding fitness value $\eta_{out} = f(x_g^{(k)})$ after the final iteration.

3.3 Coding in representing turbine locations and HGPSO optimizing

In order to facilitate optimization while maintaining the minimum distance between wind turbines, we discretize the available wind-farm surface and use the center coordinates of each grid cell as a candidate turbine location. Let

$$\Omega = \left\{x \in \{1, \dots, I_r I_c\}^D \mid x_p \neq x_q\ (p \neq q),\ x_p \notin CL\right\} \tag{23}$$

denote the feasible discrete search space. Therefore, the optimization process is discrete because HGPSO searches over feasible grid indices. For a WFLOP solution $x_i^{(k)} \in \Omega$ provided by HGPSO in generation k, we define the encoding operator

$$E(x_i^{(k)}) = \{(M_{i,1}, N_{i,1}), \dots, (M_{i,D}, N_{i,D})\}, \tag{24}$$

where the two-dimensional turbine coordinates are obtained as follows:

$$M_{i,j} = (x_{i,j} - I_r \cdot \lfloor \frac{x_{i,j} - 1}{I_r} \rfloor - 0.5) \cdot W_t \tag{25}$$

$$N_{i,j} = (\lfloor \frac{x_{i,j} - 1}{I_r} \rfloor + 0.5) \cdot W_t \tag{26}$$

where, W_t is the width of one grid cell. In the benchmark setting used in this paper, $W_t = 77 \times 3 = 231$ m. Since the rotor diameter is 77 m, this grid width guarantees that adjacent grid centers are separated by three rotor diameters. Hence, if all turbine indices are distinct, no two turbines can violate the minimum inter-turbine spacing constraint. This grid encoding therefore prevents infeasible placements before rotation and avoids repeated pairwise spacing checks during the evolutionary process. Additionally, to simulate different wind directions θ under various wind conditions in WFLOP, these turbine coordinates are rotated only for wake evaluation:

$$\begin{bmatrix} M_{i,j}^{\theta} \\ N_{i,j}^{\theta} \end{bmatrix} = \begin{bmatrix} cos(\theta) & -sin(\theta) \\ sin(\theta) & cos(\theta) \end{bmatrix} \begin{bmatrix} M_{i,j} \\ N_{i,j} \end{bmatrix} \tag{27}$$

where, $M_{i,j}^{\theta}$ and $N_{i,j}^{\theta}$ represent the rotated coordinates of wind turbine $x_{i,j}$ under wind direction θ. This definition makes the hybrid search structure explicit: HGPSO optimizes a discrete solution $x \in \Omega$, whereas the wake model evaluates the continuous geometric image $R(\theta)E(x)$. In other words, the decision space is discrete but the physical wake computation is continuous. This hybrid discrete–continuous formulation is mathematically well-defined because $E(\cdot)$ is a deterministic mapping from the finite feasible index set to continuous coordinates, and the objective function is evaluated on the mapped coordinates rather than on free continuous design variables.

Although the grid-based representation improves feasibility control and reproducibility, it may also introduce a

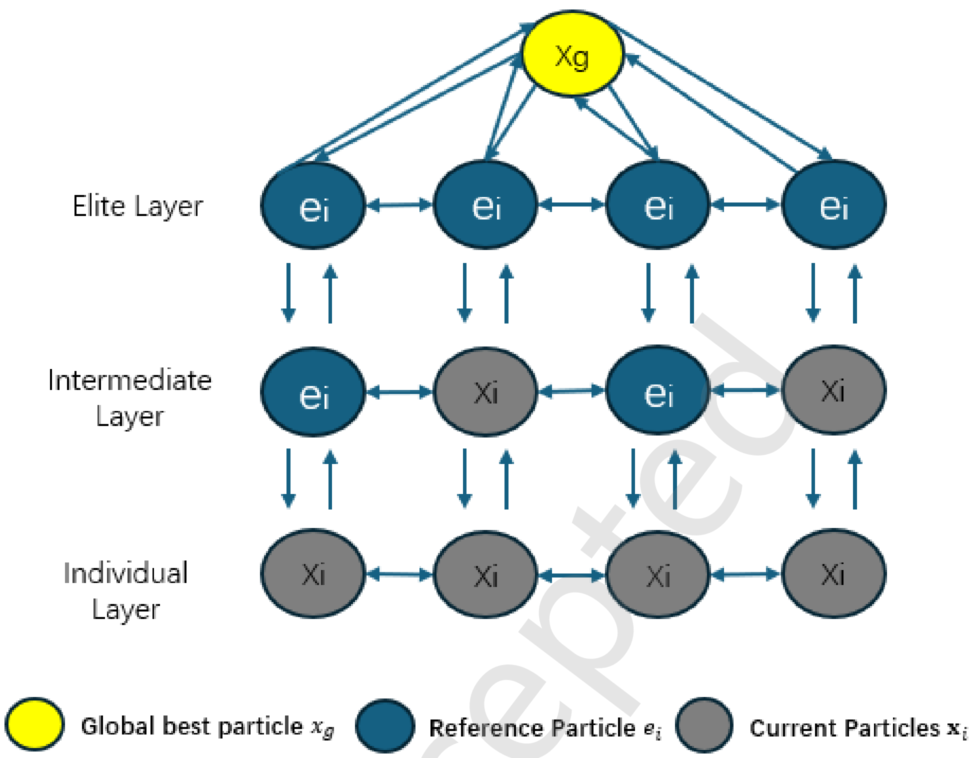

Fig. 6 Illustration of the hierarchical population structure of HGPSO.

discretization effect. Since turbines can only be placed at predefined grid-cell centers, some feasible positions in the continuous wind-farm area are not included in the search space. Therefore, the obtained solution should be interpreted as the optimum or near-optimum within the adopted discrete benchmark space rather than the theoretical optimum over all possible continuous coordinates. Nevertheless, this representation is appropriate for the purpose of this study. First, it is consistent with the open-source WFLOP benchmark platform used by the compared algorithms, which ensures fair and reproducible comparison. Second, the grid-cell width is set to three rotor diameters, so distinct grid indices naturally satisfy the minimum inter-turbine spacing requirement. Third, all algorithms are tested under the same discretized search space; therefore, the relative performance comparison mainly reflects the search capability of the optimizers rather than differences in representation. Future extensions of HGPSO may consider finer grid resolutions or continuous-coordinate optimization to further reduce discretization effects.

It should be noted that the rotation operation in Eq. (27) is introduced solely to simulate different wind directions when evaluating wake interactions and power generation. The rotation is applied only within the aerodynamic evaluation process and does not modify the actual physical layout of turbines in the wind farm. All turbine position constraints, including wind-farm boundaries, duplicate placements, and restricted zones, are enforced in the original coordinate system through the boundary detection mechanism in Eq. (20). Therefore, the feasibility of turbine locations is always verified prior to rotation, and the rotation operation cannot move turbines into prohibited regions. Because each decision dimension in x stores a homogeneous grid index with the same bounds $[1, I_r I_c]$, a scalar acceleration coefficient c is sufficient; dimension-wise scaling is unnecessary since the continuous coordinates are derived only during evaluation and are not optimized as heterogeneous variables. If future WFLOP extensions directly optimize heterogeneous continuous variables such as independent x-y coordinates, turbine heights, or mixed design parameters, then dimension-wise normalization would become a natural extension. However, that is outside the present index-based formulation.

4 Experiments and results

In this section, the effectiveness of HGPSO in solving WFLOP are tested. We validate the efficiency of HGPSO by statistically comparing it with eight theoretical and WFLOP state-of-the-art meta-heuristics across four different types. Among them, AGPSO [37], GLPSO [42], SUGGA [14], AGA [13], and

Table 2 The detailed parameter settings of optimizers in the experiments.

Algorithm Name	Year	Parameters
HGPSO	2026	$NP = 120, p_m = 0.01, s = 7, c = 1.49618, m = 0.9, r_w = 0.1$
AGPSO [37]	2022	$NP = 120, s = 7, c = 1.49618, p_m = 0.01$
GLPSO [42]	2015	$NP = 120, s = 7, c = 1.49618, \omega = 0.7298, p_m = 0.01$
SUGGA [14]	2019	$NP = 120, p_r = 0.5, p_m = 0.1, p_c = 0.6, p_e = 0.2$
AGA [13]	2019	$NP = 120, p_r = 0.5, p_m = 0.1, p_c = 0.6, p_e = 0.2$
CGA [13]	2019	$NP = 120, p_r = 0.5, p_m = 0.1, p_c = 0.6, p_e = 0.2$
SHADE [50]	2013	$NP = 120, m_s = 5, A_r = 1.4, p = 0.01$
IMODE [51]	2020	$NP_{init} = 18 \cdot D, p = 0.01, A_r = 1.4, m_s = 5$
SSM [52]	2023	$NP_{init} = 18 \cdot D, p = 0.01, A_r = 1.4, m_s = 5, \epsilon = 0.01$

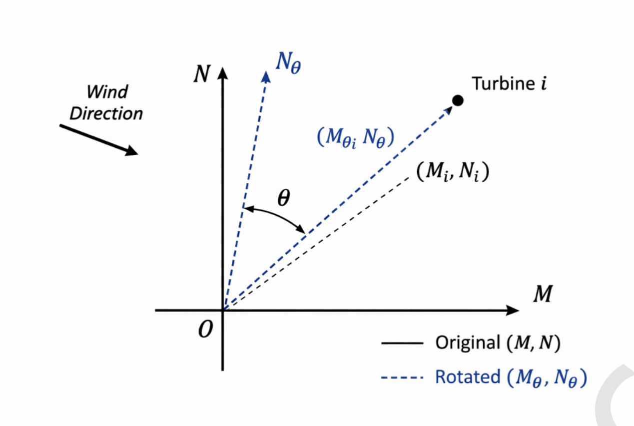

Fig. 7 Illustration of turbine coordinates before and after the computational rotation used for wake evaluation.

CGA [13] are the latest state-of-the-art methods specifically proposed for solving WFLOP in Ju et al.'s WFLOP library. SHADE, as a state-of-the-art for theoretical test sets, has been proven to perform stably and excellently in various practical problems [50, 53]. IMODE was shown to achieve the best theoretical optimization performance in the IEEE2020 competition [51]. SSM, as a new search paradigm (spherical search), was proven in 2024 to surpass most other types of state-of-the-art meta-heuristics in theoretical and practical performance and generalizability [52]. Their parameters are all set to the recommended values from the original papers, as detailed in Table 2. We present the statistical data results of the energy conversion efficiency of HGPSO and these competitors under all different combinations of four wind scenarios, three turbine quantities, and thirteen wind farm land use conditions. To provide a structured overview of representative WFLOP optimization approaches and establish the research background, Table 2 summarizes state-of-the-art algorithms considered in this study, including PSO variants, genetic algorithm–based methods, and advanced metaheuristic optimizers. This comparison offers a meta-level perspective on existing approaches and helps clarify the research gap motivating the proposed HGPSO. Additionally, the optimization convergence plots, box plots of optimization results, and visualizations of the output WFLOP solutions of all tested algorithms are provided to further analyze and verify the advantages of HGPSO.

4.1 Experimental setting

The fundamental parameters of the wind turbines and the wind farm are presented in Table 4, where the hub height and rotor diameter are set to 80 m and 77 m, respectively, the grid-cell width is fixed to $W_t = 231$ m, and the surface roughness is set to 2.5×10^{-4}. To fairly allocate computational resources, a maximum evaluation number $maxFEs = 24000$ is fixed and used for all algorithms in all experiments reported in this paper. Therefore, AGPSO, HGPSO, and all competitors are compared under the same FE budget. Due to the inherent randomness of the tested algorithms, each algorithm is independently tested 51 times to reduce random effects. To maximize the generalizability of the experimental results, four different wind scenarios are used for testing: wind scenario 1 with a single wind direction and speed, wind scenario 2 with a single wind speed and uniform multi-direction, wind scenario 3 with a single wind speed and non-uniform multi-direction, and wind scenario 4 with multiple wind speeds and directions. The wind rose graphs and specific parameters of these four wind scenarios are presented in Fig. 8 and Table 3. For each wind scenario, 13 different land-use conditions are tested, including one with no turbine exclusion zones and 12 considering multiple turbine exclusion zones due to landowner participation, with the total land area set to 12×12. As shown in Fig. 9, Constraints 1 to 6 each have 12 unusable areas, and Constraints 7 to 12 each have 24 unusable areas. Additionally, for each specific wind scenario and wind-farm land-use condition, WFLOP is tested under three different turbine-acquisition schemes with maximum turbine numbers of 15, 20, and 25. Therefore, the total number of tested WFLOPs is $4 \times 13 \times 3 = 156$. In addition, these 156 instances are controlled benchmark

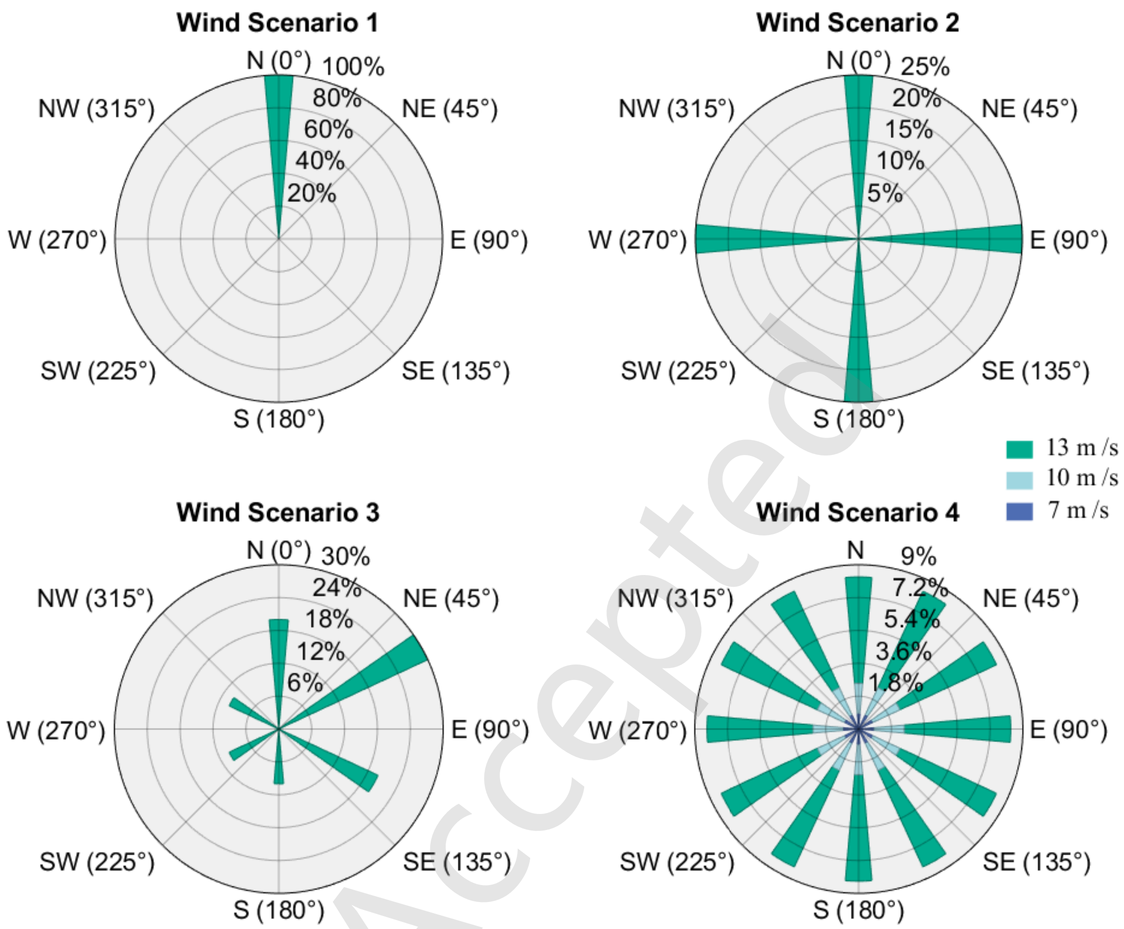

Fig. 8 Wind rose graph of the 4 types of wind distributions.

Table 3 The parameters in the 4 types of wind scenarios.

	Speed	0°	30°	60°	90°	120°	150°	180°	210°	240°	270°	300°	330°
WS1	13 m/s	100%	–	–	–	–	–	–	–	–	–	–	–
WS2	13 m/s	25%	–	–	25%	–	–	25%	–	–	25%	–	–
WS3	13 m/s	20%	–	30%	–	20%	–	10%	–	10%	–	10%	
	7 m/s	0.83%	0.83%	0.83%	0.83%	0.83%	0.83%	0.83%	0.83%	0.83%	0.83%	0.83%	0.83%
WS4	10 m/s	1.67%	1.67%	1.67%	1.67%	1.67%	1.67%	1.67%	1.67%	1.67%	1.67%	1.67%	1.67%
	13 m/s	5.83%	5.83%	5.83%	5.83%	5.83%	5.83%	5.83%	5.83%	5.83%	5.83%	5.83%	5.83%

Table 4 The fundamental parameters of the wind turbines and the wind farm.

Wind Farm Parameters	**Value**
Height of hub (m)	80
Diameter of rotor (m)	77
Grid-cell width W_t (m)	231
Roughness of surface	2.5×10^{-4}

cases rather than site-specific real-world wind farm cases. Although the four wind scenarios and thirteen land-use conditions increase the diversity of the test environment, they do not explicitly incorporate real-world terrain variability, such as elevation changes, irregular ground surfaces, or spatially varying roughness. The wind conditions are also represented by predefined wind-speed and wind-direction probability settings, rather than stochastic uncertainty models derived from long-term measured wind data. Therefore, the experimental results should be interpreted within the adopted benchmark framework, while the behavior of HGPSO under more realistic terrain and wind-uncertainty conditions remains to be further investigated. The results obtained by the Wilcoxon

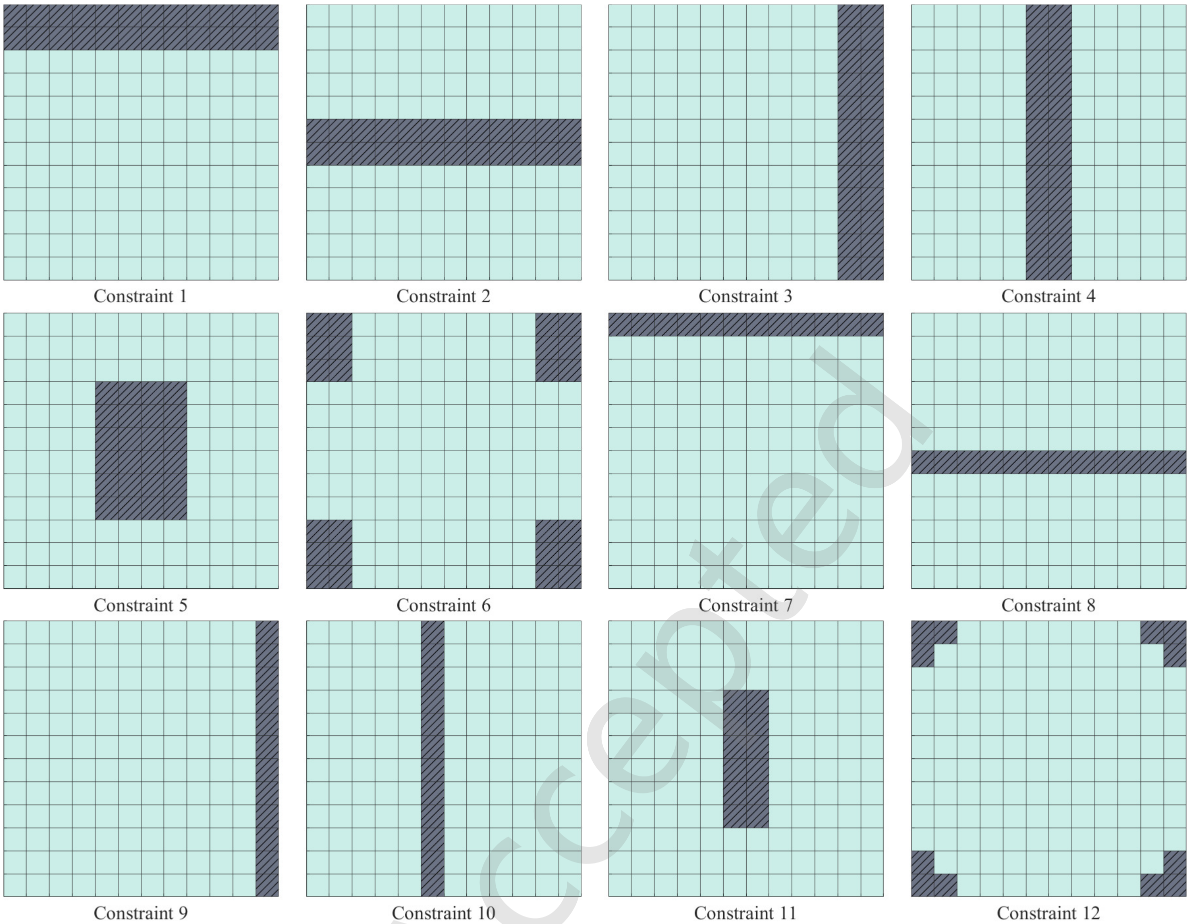

Fig. 9 Illustration of the 13 land-use constraint patterns used in the WFLOP experiments.

rank-sum test [54, 55] for HGPSO against each competing algorithm are presented in Tables 5-12, where Constraints 1 to 12 correspond to Problems 2 to 13. It should be noted that the turbine numbers tested in this study follow the adopted benchmark WFLOP setting, namely N=15, 20, and 25. These settings are suitable for evaluating the search behavior of different optimizers under controlled benchmark conditions and ensure fair comparison with existing benchmark algorithms. However, they do not fully represent very large-scale wind farms with hundreds of turbines. Therefore, the present results should be interpreted as benchmark-scale validation of HGPSO, while its performance on very large-scale WFLOP remains to be further investigated. This non-parametric statistical test is employed to evaluate whether the performance differences between HGPSO and each competing algorithm are statistically significant without assuming normal data distribution. Since the statistical validation in this study focuses on pairwise comparisons between HGPSO and each competitor on each WFLOP instance, the Wilcoxon rank-sum test is adopted. At a significance level of p=0.05, HGPSO is considered significantly better, comparable, or inferior to a competing method, which are denoted by Win "+", Tie "=", and Lose "–", respectively. In addition to the hypothesis test, the mean values, standard deviations, and $W/T/L$ summaries are jointly reported to describe the magnitude, stability, and overall trend of the performance differences. All experiments are based on MATLAB R2022b on a PC with 16 GB RAM and an Intel(R) Core(TM) i7-12700KF. The source code of HGPSO will be provided at http://toyamaailab.github.io/.

To provide a clearer comparison between HGPSO and competing algorithms, both convergence behavior and solution quality are analyzed using multiple performance indicators. The convergence plots illustrate the optimization dynamics and convergence speed of different algorithms during the search process, while the boxplot distributions present the statistical characteristics of solution quality and robustness over independent runs. These figures enable a direct comparison between HGPSO and AGPSO in terms of convergence efficiency and stability. In addition to solution quality, the cost–performance relationship should also be considered. In all experiments, the maximum number of function evaluations is fixed to maxFEs=24000 for each algorithm. Therefore, the reported performance improvements of HGPSO are obtained under the same objective-function evaluation budget as the compared methods. The additional optimizer-side cost mainly comes from the case-based level-direction guided update in Eq. (22), which involves only a constant number of conditional comparisons and arithmetic operations for each decision dimension. Since WFLOP fitness evaluation requires wake-effect calculation and power evaluation, the total runtime is still dominated by the objective-function evaluation rather than by the additional update logic. Thus, the observed improvement of approximately 0.5%–3.0% can be interpreted as a gain achieved with limited extra optimizer-side overhead under the adopted benchmark setting.

In addition, the convergence curves, boxplot distributions, standard deviations, and statistical comparison results are jointly used to analyze the exploration–exploitation behavior of the tested algorithms. In this study, convergence speed and later-stage improvement reflect the exploitation ability of an algorithm, while stable solution distributions over 51 independent runs indicate whether the algorithm can maintain reliable search behavior instead of prematurely converging to unstable local optima. From this perspective, the exploration–exploitation trade-off can be assessed by considering the convergence trajectories, final solution distributions, and statistical robustness together. The convergence plots show that HGPSO usually maintains continuous improvement during the search process, especially in constrained and higher-dimensional WFLOP cases. Meanwhile, the boxplot results and statistical comparisons show that HGPSO obtains stable final solutions in most tested scenarios. These observations suggest that the hierarchical guidance mechanism helps HGPSO exploit promising regions while preserving effective search capability under the fixed function-evaluation budget.

4.2 Statistical results under the wind scenario 1

In a wind scenario 1 with a single wind speed and single wind direction (v = 13 m/s, $\theta = 0°$), HGPSO and other competing algorithms were tested. Table 5 and Table 6 present the optimization results of 51 independent experiments, including the mean value, standard deviation, and statistical results (Wilcoxon Rank-sum Test) for the conversion efficiency of solutions corresponding to different algorithms.

From Table 5, it can be seen that when the number of turbines is 15, 20, and 25, HGPSO obtains better results than AGPSO in 6, 9, and 4 problems, respectively, totaling 19 problems, and shows comparable performance to AGPSO in the other 20 problems. While being comparable in the remaining cases, suggesting that the proposed operator can serve as an effective alternative to AGPSO in this scenario. Additionally, HGPSO shows significant advantages over all four state-of-the-art WFLOP algorithms. Compared to GLPSO, HGPSO achieves significantly better solutions in all problems. Although HGPSO achieves only a 5/2/6 W/T/L result compared to SUGGA in the 15-turbine problems, it outperforms SUGGA in most of the 20 and 25-turbine problems. HGPSO shows significant advantages over AGA in 32 problems and is inferior in most of the remaining 7 problems. This observation suggests that SUGGA and AGA remain competitive in certain settings, whereas their performance may vary across different WFLOP configurations.

Table 6 includes other algorithms with advanced WFLOP and theoretical performance. It can be seen that HGPSO is inferior to SHADE and IMODE in 1 and 3 problems, respectively, but outperforms them in most problems (33 and 28, respectively). Compared to CGA and SSM, HGPSO remains unbeaten in all 39 problems and significantly outperforms them in 27 and 39 problems, respectively. Another noteworthy point is that HGPSO shows a positive performance trend in higher-dimensional problems with 20 and 25 turbines (usually implying more complex solution spaces). Therefore, compared to these competing algorithms, HGPSO demonstrates stronger adaptability to complex WFLOPs.

Fig. 10 shows the average convergence process of all tested algorithms in solving three WFLOPs (with turbine numbers $N = 15, 20, 25$ and constraint types $C = 11, 5, 0$) over 51 independent optimizations. From Fig. 10, it can be seen that HGPSO has a significantly faster convergence speed within a certain time frame, meaning it can find better solutions compared to other algorithms under the same time threshold. This indicates that HGPSO outperforms all or most competing algorithms (depending on the specific computational and time resources) with fewer computational resources. Fig. 11 shows the box plot graphs for the three WFLOPs. It can be seen that HGPSO has a higher mean conversion efficiency in multiple optimization results compared to all competitors, while also maintaining excellent robustness. This demonstrates that HGPSO can find high-quality WFLOP solutions more stably.

Fig. 12 shows an example with 25 turbines and no turbine placement constraints. It can be seen that under a single wind direction ($\theta = 0°$) north wind at a constant speed, the turbines optimized by HGPSO are arranged more neatly at the north and south ends of the wind farm compared to other competitors. We can intuitively sense that the turbines on the south side are less affected by the wake effect from the turbines on the north side, and the wind farm maximizes the utilization of wind energy. Therefore, the solution provided

Table 5 The comparison results of HGPSO and other competitors in wind scenario 1 in solving WFLOP under turbine number of 15, 20, and 25.

Turbine	Problem	HGPSO		AGPSO			GLPSO			SUGGA			AGA		
		Mean	SD	Mean	SD	W	Mean	SD	W	Mean	SD	W	Mean	SD	W
15	1	97.84%	0.09%	97.81%	0.10%	+	97.66%	0.21%	+	97.81%	0.09%	+	97.69%	0.11%	+
	2	96.90%	0.13%	96.89%	0.11%	=	96.85%	0.14%	+	97.24%	0.22%	-	97.06%	0.24%	+
	3	97.85%	0.09%	97.83%	0.09%	=	97.80%	0.12%	+	97.84%	0.07%	=	97.75%	0.11%	+
	4	96.32%	0.17%	96.17%	0.25%	+	95.98%	0.35%	+	97.70%	0.32%	-	97.49%	0.36%	+
	5	96.28%	0.23%	96.20%	0.24%	+	95.99%	0.28%	+	97.44%	0.46%	-	97.45%	0.39%	=
	6	97.88%	0.05%	97.84%	0.10%	+	97.82%	0.11%	+	97.83%	0.08%	+	97.76%	0.10%	+
	7	97.81%	0.13%	97.74%	0.13%	+	97.66%	0.20%	+	97.77%	0.11%	+	97.56%	0.18%	+
	8	97.41%	0.12%	97.39%	0.11%	=	97.29%	0.19%	+	97.51%	0.12%	-	97.40%	0.15%	+
	9	97.83%	0.10%	97.83%	0.10%	=	97.75%	0.14%	+	97.81%	0.09%	+	97.68%	0.12%	+
	10	97.02%	0.17%	96.99%	0.20%	=	96.92%	0.20%	+	97.80%	0.15%	-	97.57%	0.31%	=
	11	97.04%	0.17%	97.03%	0.17%	=	96.85%	0.29%	+	97.65%	0.33%	-	97.61%	0.25%	+
	12	97.85%	0.08%	97.81%	0.11%	+	97.77%	0.14%	+	97.81%	0.08%	+	97.70%	0.12%	+
	13	97.74%	0.16%	97.75%	0.17%	=	97.57%	0.26%	+	97.76%	0.11%	=	97.55%	0.16%	+
	W/T/L	–/–/–		6/7/0			13/0/0			5/2/6			8/0/5		
Turbine	Problem	HGPSO		AGPSO			GLPSO			SUGGA			AGA		
		Mean	SD	Mean	SD	W	Mean	SD	W	Mean	SD	W	Mean	SD	W
20	1	94.96%	0.40%	94.95%	0.40%	=	94.56%	0.48%	+	94.19%	0.45%	+	93.59%	0.52%	+
	2	93.19%	0.35%	93.04%	0.43%	+	92.76%	0.49%	+	92.61%	0.54%	+	92.03%	0.61%	+
	3	95.27%	0.24%	95.14%	0.33%	+	95.04%	0.29%	+	94.51%	0.25%	+	93.99%	0.34%	+
	4	93.57%	0.42%	93.15%	0.61%	+	92.38%	0.67%	+	94.18%	0.44%	-	93.00%	0.91%	+
	5	93.43%	0.42%	93.15%	0.45%	+	92.52%	0.56%	+	93.28%	0.87%	=	92.92%	0.76%	+
	6	95.36%	0.23%	95.24%	0.24%	+	95.07%	0.29%	+	94.60%	0.27%	+	94.13%	0.38%	+
	7	94.78%	0.51%	94.29%	0.64%	+	94.13%	0.52%	+	93.28%	0.66%	+	92.21%	0.63%	+
	8	94.12%	0.36%	94.10%	0.36%	=	93.75%	0.41%	+	93.47%	0.41%	+	92.88%	0.50%	+
	9	95.24%	0.36%	95.05%	0.32%	+	94.92%	0.36%	+	94.37%	0.32%	+	93.80%	0.55%	+
	10	94.26%	0.47%	94.18%	0.40%	=	93.56%	0.56%	+	94.34%	0.44%	=	93.24%	0.61%	+
	11	94.29%	0.43%	94.10%	0.40%	+	93.66%	0.52%	+	93.86%	0.54%	+	93.10%	0.68%	+
	12	95.16%	0.33%	95.17%	0.28%	=	94.93%	0.38%	+	94.42%	0.32%	+	93.82%	0.36%	+
	13	94.56%	0.49%	94.34%	0.49%	+	94.06%	0.62%	+	93.50%	0.41%	+	92.78%	0.62%	+
	W/T/L	–/–/–		9/4/0			13/0/0			10/2/1			13/0/0		
Turbine	Problem	HGPSO		AGPSO			GLPSO			SUGGA			AGA		
		Mean	SD	Mean	SD	W	Mean	SD	W	Mean	SD	W	Mean	SD	W
25	1	91.09%	0.55%	90.94%	0.45%	=	90.32%	0.64%	+	88.34%	0.54%	+	87.68%	0.71%	+
	2	88.32%	0.59%	88.34%	0.48%	=	87.81%	0.65%	+	86.03%	0.97%	+	85.15%	0.79%	+
	3	91.44%	0.39%	91.36%	0.46%	=	90.77%	0.65%	+	88.81%	0.58%	+	88.06%	0.74%	+
	4	84.46%	0.39%	84.26%	0.37%	+	83.91%	0.48%	+	87.92%	0.87%	-	86.29%	1.01%	+
	5	84.48%	0.33%	84.30%	0.48%	+	83.87%	0.46%	+	86.63%	1.21%	-	86.48%	1.00%	+
	6	91.63%	0.36%	91.60%	0.30%	=	91.05%	0.53%	+	88.85%	0.62%	+	88.30%	0.70%	+
	7	87.77%	0.55%	87.46%	0.46%	+	86.94%	0.60%	+	86.75%	0.87%	+	85.06%	1.00%	+
	8	89.78%	0.60%	89.87%	0.51%	=	89.22%	0.59%	+	87.27%	0.75%	+	86.50%	0.67%	+
	9	91.31%	0.44%	91.27%	0.41%	=	90.57%	0.56%	+	88.63%	0.63%	+	87.83%	0.66%	+
	10	87.98%	0.40%	87.79%	0.41%	+	87.39%	0.47%	+	88.49%	0.86%	-	87.12%	0.89%	+
	11	87.87%	0.42%	87.81%	0.37%	=	87.34%	0.57%	+	87.56%	1.12%	+	87.22%	0.75%	+
	12	91.36%	0.43%	91.25%	0.45%	=	90.91%	0.45%	+	88.70%	0.57%	+	87.93%	0.59%	+
	13	89.76%	0.50%	89.62%	0.58%	=	88.92%	0.61%	+	87.44%	0.73%	+	86.27%	0.74%	+
	W/T/L	–/–/–		4/9/0			13/0/0			10/0/3			11/0/2		
Total	W/T/L	–/–/–		19/20/0			39/0/0			25/4/10			32/0/7		

by HGPSO achieves the highest energy conversion efficiency in this example. This validates the basic understanding and implementation of the wake effect in the experiment, and also indicates that HGPSO can find more reasonable WFLOP solutions.

4.3 Statistical results under the wind scenario 2

In a wind scenario 2 with a single wind speed and four uniform wind directions (v = 13 m/s, $\theta = 0°, 90°, 180°, 270°$), HGPSO and other competing algorithms were tested. Table 7 and Table 8 present the optimization results of 51 independent experiments, including the mean, standard deviation, and Wilcoxon rank-sum test statistical results for the conversion efficiency of solutions corresponding to different algorithms.

From Table 7, it can be seen that when the number of turbines is 15, 20, and 25, HGPSO is significantly better than AGPSO in 4, 8, and 11 problems, respectively, totaling 23 problems, and shows comparable performance to AGPSO in the other 16 problems. This further indicates that the level-direction guided hierarchical PSO operator proposed in this paper effectively advances the performance of PSO variants in solving WFLOP. Compared to the other three WFLOP state-of-the-art algorithms, HGPSO shows significant advantages,

Table 6 The comparison results of HGPSO and other competitors in wind scenario 1 in solving WFLOP under turbine number of 15, 20, and 25.

Turbine	Problem	HGPSO		CGA			SHADE			IMODE			SSM		
		Mean	SD	Mean	SD	W	Mean	SD	W	Mean	SD	W	Mean	SD	W
15	1	97.84%	0.09%	97.35%	0.24%	+	97.80%	0.13%	+	97.86%	0.06%	=	95.48%	0.56%	+
	2	96.90%	0.13%	96.60%	0.32%	+	96.92%	0.08%	=	96.95%	0.05%	-	94.63%	0.68%	+
	3	97.85%	0.09%	97.53%	0.18%	+	97.88%	0.03%	-	97.89%	0.02%	-	96.59%	0.42%	+
	4	96.32%	0.17%	95.80%	0.77%	+	95.93%	0.19%	+	96.06%	0.18%	+	92.25%	0.70%	+
	5	96.28%	0.23%	96.11%	0.78%	=	95.93%	0.22%	+	96.07%	0.17%	+	92.45%	0.87%	+
	6	97.88%	0.05%	97.55%	0.17%	+	97.88%	0.05%	=	97.89%	0.02%	=	96.20%	0.73%	+
	7	97.81%	0.13%	97.16%	0.30%	+	97.59%	0.16%	+	97.81%	0.08%	=	94.47%	0.76%	+
	8	97.41%	0.12%	96.93%	0.29%	+	97.38%	0.18%	=	97.45%	0.06%	=	95.03%	0.70%	+
	9	97.83%	0.10%	97.50%	0.21%	+	97.87%	0.05%	=	97.87%	0.05%	-	96.03%	0.53%	+
	10	97.02%	0.17%	96.80%	0.62%	=	96.98%	0.11%	+	97.06%	0.11%	=	94.19%	0.70%	+
	11	97.04%	0.17%	96.60%	0.60%	+	96.92%	0.13%	+	97.03%	0.10%	=	94.16%	0.82%	+
	12	97.85%	0.08%	97.51%	0.22%	+	97.87%	0.05%	=	97.87%	0.05%	=	95.77%	0.66%	+
	13	97.74%	0.16%	97.14%	0.35%	+	97.64%	0.13%	+	97.79%	0.08%	=	95.10%	0.67%	+
	W/T/L	–/–/–		11/2/0			7/5/1			2/8/3			13/0/0		
Turbine	Problem	HGPSO		CGA			SHADE			IMODE			SSM		
		Mean	SD	Mean	SD	W	Mean	SD	W	Mean	SD	W	Mean	SD	W
20	1	94.96%	0.40%	92.30%	0.70%	+	93.60%	0.51%	+	93.79%	0.47%	+	88.04%	0.95%	+
	2	93.19%	0.35%	90.55%	0.86%	+	91.58%	0.76%	+	91.87%	0.51%	+	86.29%	1.01%	+
	3	95.27%	0.24%	93.11%	0.67%	+	94.72%	0.26%	+	94.43%	0.34%	+	89.98%	0.74%	+
	4	93.57%	0.42%	89.92%	1.24%	+	90.23%	0.96%	+	90.21%	0.72%	+	83.39%	1.05%	+
	5	93.43%	0.42%	89.82%	1.30%	+	90.08%	0.83%	+	90.15%	0.70%	+	83.56%	0.98%	+
	6	95.36%	0.23%	93.27%	0.81%	+	94.86%	0.30%	+	94.44%	0.25%	+	89.03%	1.06%	+
	7	94.78%	0.51%	90.56%	0.73%	+	91.58%	0.65%	+	92.28%	0.53%	+	86.08%	1.08%	+
	8	94.12%	0.36%	91.52%	0.79%	+	92.74%	0.41%	+	92.90%	0.47%	+	87.19%	0.79%	+
	9	95.24%	0.36%	92.80%	0.56%	+	94.27%	0.42%	+	94.16%	0.39%	+	89.11%	0.80%	+
	10	94.26%	0.47%	91.30%	1.06%	+	92.24%	0.49%	+	92.24%	0.47%	+	86.28%	1.05%	+
	11	94.29%	0.43%	91.20%	1.04%	+	92.26%	0.54%	+	92.47%	0.57%	+	85.88%	1.01%	+
	12	95.16%	0.33%	92.58%	0.61%	+	94.46%	0.33%	+	94.07%	0.42%	+	88.49%	1.00%	+
	13	94.56%	0.49%	91.36%	0.70%	+	92.40%	0.53%	+	92.97%	0.43%	+	86.96%	1.02%	+
	W/T/L	–/–/–		13/0/0			13/0/0			13/0/0			13/0/0		
Turbine	Problem	HGPSO		CGA			SHADE			IMODE			SSM		
		Mean	SD	Mean	SD	W	Mean	SD	W	Mean	SD	W	Mean	SD	W
25	1	91.09%	0.55%	85.81%	0.65%	+	87.59%	0.61%	+	86.98%	0.62%	+	80.58%	0.90%	+
	2	88.32%	0.59%	83.41%	0.86%	+	84.73%	0.91%	+	84.09%	0.77%	+	78.36%	1.15%	+
	3	91.44%	0.39%	86.42%	0.69%	+	89.42%	0.69%	+	88.13%	0.82%	+	82.90%	0.95%	+
	4	84.46%	0.39%	82.73%	1.75%	+	81.96%	0.42%	+	81.09%	0.59%	+	75.28%	0.87%	+
	5	84.48%	0.33%	83.06%	1.52%	+	81.76%	0.89%	+	81.18%	0.59%	+	75.24%	0.85%	+
	6	91.63%	0.36%	86.49%	0.82%	+	89.42%	1.08%	+	88.06%	0.68%	+	81.49%	0.90%	+
	7	87.77%	0.55%	83.47%	0.80%	+	84.01%	0.67%	+	83.82%	0.60%	+	77.81%	0.83%	+
	8	89.78%	0.60%	84.76%	0.82%	+	86.25%	0.77%	+	85.76%	0.66%	+	79.32%	0.78%	+
	9	91.31%	0.44%	86.45%	0.69%	+	88.81%	0.76%	+	87.54%	0.66%	+	81.82%	0.77%	+
	10	87.98%	0.40%	84.23%	1.38%	+	85.04%	0.50%	+	84.32%	0.70%	+	78.00%	0.78%	+
	11	87.87%	0.42%	84.29%	1.37%	+	84.86%	0.75%	+	84.41%	0.68%	+	78.16%	0.87%	+
	12	91.36%	0.43%	86.01%	0.62%	+	88.83%	0.60%	+	87.46%	0.70%	+	80.95%	0.78%	+
	13	89.76%	0.50%	84.76%	0.85%	+	86.01%	0.52%	+	85.61%	0.73%	+	79.14%	0.94%	+
	W/T/L	–/–/–		13/0/0			13/0/0			13/0/0			13/0/0		
Total	W/T/L	–/–/–		37/2/0			33/5/1			28/8/3			39/0/0		

achieving total W/T/L results of 39/0/0, 33/1/5, and 33/1/5, respectively. The results in Table 8 show that compared to CGA, SHADE, IMODE, and SSM, HGPSO outperforms them in all 39 WFLOPs. These results indicate that in wind scenario 2, HGPSO continues to perform excellently and can significantly advance the performance frontier of PSO variants in WFLOP, outperforming other algorithms with strong theoretical performance.

Fig. 13 shows the average convergence process of all tested algorithms in solving three WFLOPs (with turbine numbers $N = 15, 20, 25$ and constraint types $C = 9, 8, 11$) over 51 independent optimizations. From Fig. 13, it can be seen that after approximately 50 iterations, HGPSO begins to maintain a significant convergence advantage in all three turbine dimension problems. This means that at the 50-iteration mark, HGPSO has the fastest convergence speed to obtain better solutions. This property remains valid with more computational resources (more than 50 iterations). Furthermore, among these competitors, at any time point, HGPSO's solutions are among the best. Fig. 14 shows the box plot graphs for these three WFLOPs. It can be seen that HGPSO also demonstrates high mean and excellent robustness in wind scenario 2.

Fig. 15 shows a WFLOP example with 15 turbines under

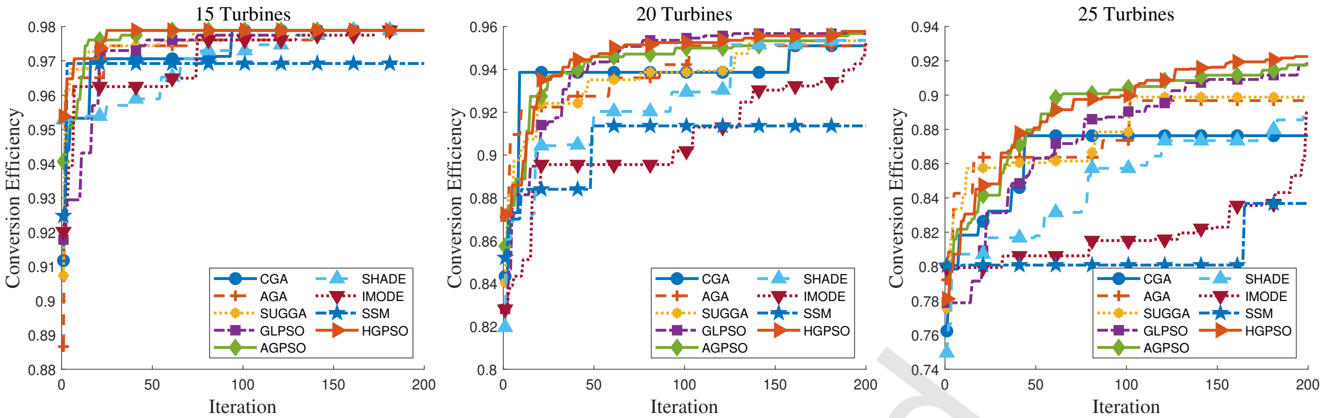

Fig. 10 The convergence plot of HGPSO compared with other competitors in wind scenario 1.

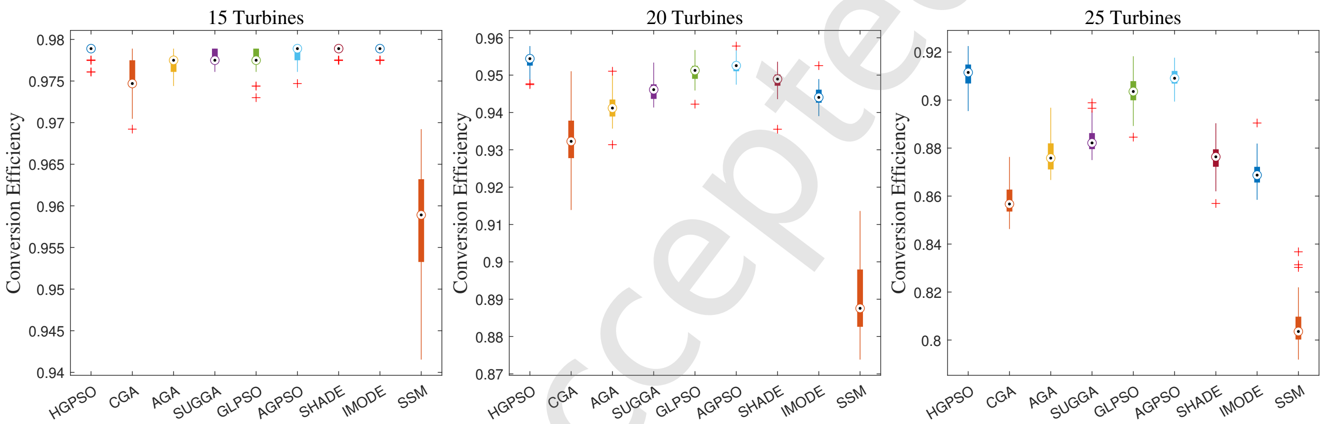

Fig. 11 The boxplot of HGPSO compared with other competitors in wind scenario 1.

Constraint 9. It can be seen that in the uniform four-wind-direction wind scenario with $\theta = 0°, 90°, 180°, 270°$, compared to other competitors, HGPSO arranges the turbines in an “x” shape rather than a “+”, to avoid continuous alignment of turbines in the direction of the wind as much as possible. This reduces the wake effect and improves wind energy conversion efficiency. Additionally, among the four types of algorithms, the three PSO variants (including GLPSO, which has not been specifically improved for WFLOP) achieved the top three solutions. This further indicates that PSO variants might be more suitable for application and further development in WFLOP. Although AGPSO made improvements to GLPSO for WFLOP, it did not break through a conversion efficiency of 0.9654 in this example, while HGPSO succeeded in surpassing this threshold.

4.4 Statistical results under the wind scenario 3

Fig. 16 shows the average convergence process of all tested algorithms in solving three WFLOPs (with turbine numbers $N = 15, 20, 25$ and constraint types $C = 5, 7, 12$) over 51 independent optimizations. From Fig. 16, it can be seen that HGPSO’s convergence speed is among the fastest. In the later stages of convergence, HGPSO is able to consistently escape local optima and find better regions in the solution space. This ability is particularly important in complex solution spaces, as higher dimensions require algorithms with population diversity characteristics to avoid local optima and stably solve complex problems [56]. This phenomenon is also evident in the convergence plot for 25 turbines. Fig. 17 shows the box plot graphs. We can see that in wind scenario 3, HGPSO exhibits higher robustness and mean conversion efficiency compared to other competitors.

Fig. 18 shows a WFLOP example with 25 turbines under Constraint 12. A notable feature is that the optimized results of HGPSO are significantly more orderly compared to other PSO variants and other competitors, resulting in the highest energy conversion rate among them. This indicates that HGPSO does not miss simple, reasonable, and efficient wind farm layout solutions. Such a layout not only features high conversion efficiency but also makes turbine construction more convenient. Additionally, it allows for large and contiguous areas to be reserved for transportation, construction,

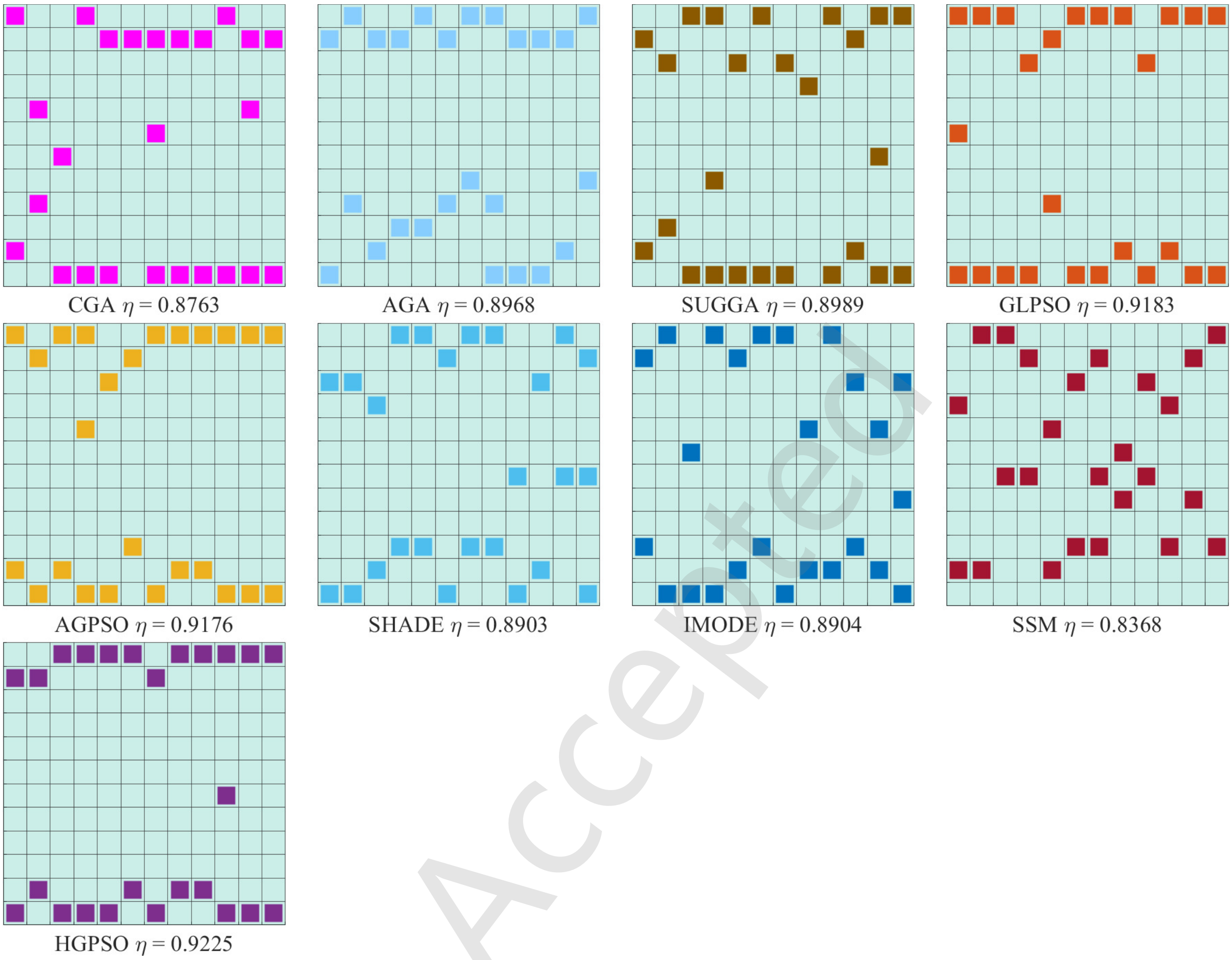

Fig. 12 The visualization of WFLOP solutions obtained from HGPSO and other competitors in wind scenario 1.

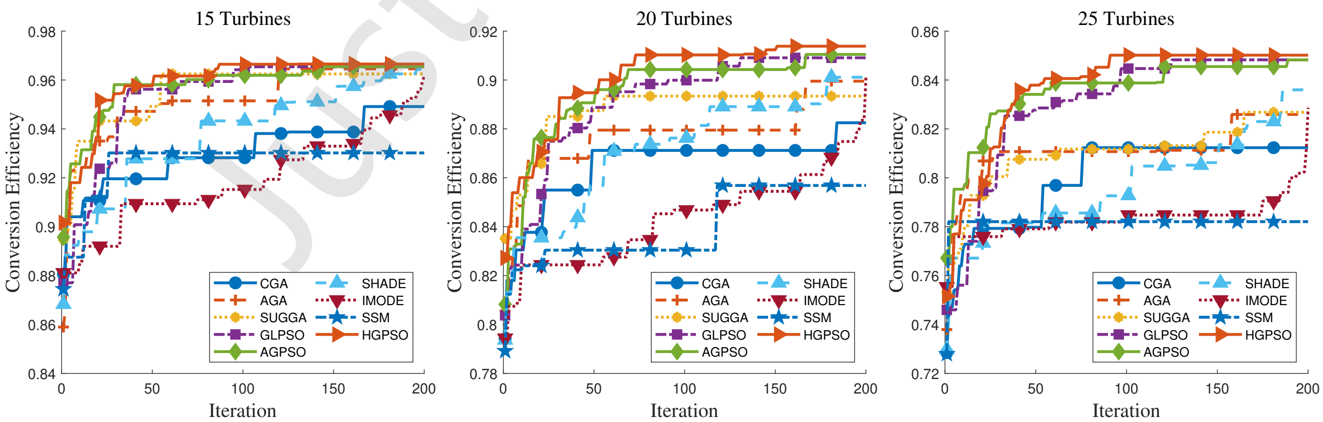

Fig. 13 The convergence plot of HGPSO compared with other competitors in wind scenario 2.

and other potential agricultural uses, maximizing land use efficiency. This characteristic of HGPSO's solutions is evident in Fig. 12, Fig. 15, Fig. 18, and Fig. 21, and is particularly noticeable under complex wind conditions in the latter two cases, which also include various land use constraints due to landowner participation.

In a wind scenario 3 with a single wind speed and six uniform wind directions (v = 13 m/s, θ = 0°, 60°, 120°, 180°, 240°, 300° with probabilities of 0.2, 0.3, 0.2, 0.1, 0.1, and 0.1), HGPSO and other competing algorithms were tested.

Table 7 The comparison results of HGPSO and other competitors in wind scenario 2 in solving WFLOP under turbine number of 15, 20, and 25.

Turbine	Problem	HGPSO		AGPSO			GLPSO			SUGGA			AGA		
		Mean	SD	Mean	SD	W	Mean	SD	W	Mean	SD	W	Mean	SD	W
15	1	97.09%	0.23%	97.05%	0.23%	=	96.92%	0.26%	+	95.41%	0.41%	+	95.45%	0.41%	+
	2	95.00%	0.34%	94.98%	0.29%	=	94.79%	0.36%	+	95.13%	0.65%	=	95.00%	0.57%	=
	3	95.65%	0.21%	95.62%	0.25%	=	95.30%	0.32%	+	94.86%	0.59%	+	94.94%	0.53%	+
	4	94.95%	0.35%	94.89%	0.36%	=	94.65%	0.41%	+	95.44%	0.51%	-	95.41%	0.61%	-
	5	95.60%	0.24%	95.46%	0.24%	+	95.35%	0.31%	+	94.82%	0.71%	+	94.96%	0.52%	+
	6	96.56%	0.33%	96.45%	0.35%	+	96.31%	0.44%	+	94.57%	0.37%	+	94.78%	0.34%	+
	7	96.69%	0.23%	96.70%	0.23%	=	96.53%	0.30%	+	95.46%	0.45%	+	95.29%	0.33%	+
	8	96.13%	0.31%	96.12%	0.22%	=	95.95%	0.36%	+	95.60%	0.40%	+	95.59%	0.46%	+
	9	96.49%	0.21%	96.47%	0.28%	=	96.25%	0.31%	+	95.08%	0.54%	+	95.06%	0.38%	+
	10	96.20%	0.26%	96.05%	0.28%	+	95.92%	0.31%	+	95.41%	0.44%	+	95.41%	0.44%	+
	11	96.42%	0.25%	96.36%	0.27%	=	96.18%	0.26%	+	95.15%	0.53%	+	95.23%	0.47%	+
	12	97.02%	0.27%	96.86%	0.29%	+	96.70%	0.32%	+	95.22%	0.48%	+	95.23%	0.45%	+
	13	96.83%	0.16%	96.81%	0.17%	=	96.59%	0.23%	+	95.35%	0.40%	+	95.28%	0.37%	+
	W/T/L	–/–/–		4/9/0			13/0/0			11/1/1			11/1/1		
Turbine	Problem	HGPSO		AGPSO			GLPSO			SUGGA			AGA		
		Mean	SD	Mean	SD	W	Mean	SD	W	Mean	SD	W	Mean	SD	W
20	1	91.48%	0.39%	91.34%	0.42%	=	91.03%	0.52%	+	88.64%	0.43%	+	88.84%	0.46%	+
	2	87.52%	0.30%	87.53%	0.29%	=	87.23%	0.38%	+	87.97%	0.82%	-	87.79%	0.84%	-
	3	89.42%	0.24%	89.29%	0.32%	+	89.08%	0.43%	+	87.96%	0.65%	+	88.26%	0.69%	+
	4	87.56%	0.30%	87.40%	0.36%	+	87.20%	0.36%	+	88.59%	0.53%	-	88.53%	0.64%	-
	5	89.41%	0.23%	89.23%	0.28%	+	89.09%	0.38%	+	88.41%	0.65%	+	88.55%	0.55%	+
	6	89.87%	0.24%	89.65%	0.34%	+	89.63%	0.37%	+	88.00%	0.52%	+	88.09%	0.41%	+
	7	89.95%	0.38%	89.93%	0.37%	=	89.55%	0.41%	+	88.53%	0.54%	+	88.36%	0.54%	+
	8	89.72%	0.36%	89.71%	0.42%	=	89.38%	0.39%	+	88.66%	0.62%	+	88.59%	0.59%	+
	9	90.60%	0.36%	90.44%	0.33%	+	90.05%	0.33%	+	88.27%	0.47%	+	88.57%	0.48%	+
	10	89.68%	0.34%	89.50%	0.38%	+	89.31%	0.33%	+	88.54%	0.48%	+	88.49%	0.67%	+
	11	90.50%	0.39%	90.28%	0.42%	+	90.16%	0.42%	+	88.44%	0.51%	+	88.57%	0.57%	+
	12	90.83%	0.33%	90.58%	0.39%	+	90.48%	0.42%	+	88.39%	0.39%	+	88.58%	0.44%	+
	13	90.84%	0.39%	90.84%	0.39%	=	90.41%	0.46%	+	88.75%	0.41%	+	88.64%	0.44%	+
	W/T/L	–/–/–		8/5/0			13/0/0			11/0/2			11/0/2		
Turbine	Problem	HGPSO		AGPSO			GLPSO			SUGGA			AGA		
		Mean	SD	Mean	SD	W	Mean	SD	W	Mean	SD	W	Mean	SD	W
25	1	84.74%	0.24%	84.54%	0.41%	+	84.35%	0.35%	+	81.94%	0.38%	+	81.99%	0.36%	+
	2	79.81%	0.27%	79.71%	0.30%	+	79.50%	0.35%	+	80.59%	0.82%	-	80.46%	0.94%	-
	3	82.36%	0.36%	82.21%	0.30%	+	82.02%	0.33%	+	81.06%	0.81%	+	81.38%	0.68%	+
	4	79.78%	0.28%	79.57%	0.32%	+	79.56%	0.36%	+	81.68%	0.67%	-	81.44%	0.63%	-
	5	82.39%	0.28%	82.14%	0.33%	+	82.01%	0.37%	+	81.42%	0.65%	+	81.64%	0.60%	+
	6	83.49%	0.30%	83.40%	0.30%	+	83.17%	0.35%	+	81.36%	0.40%	+	81.45%	0.34%	+
	7	83.06%	0.37%	82.90%	0.41%	+	82.68%	0.39%	+	81.47%	0.50%	+	81.31%	0.59%	+
	8	82.38%	0.30%	82.30%	0.33%	=	82.07%	0.29%	+	81.57%	0.62%	+	81.58%	0.57%	+
	9	83.63%	0.30%	83.49%	0.36%	+	83.22%	0.40%	+	81.56%	0.55%	+	81.74%	0.49%	+
	10	82.39%	0.33%	82.17%	0.29%	+	82.07%	0.35%	+	81.72%	0.48%	+	81.62%	0.49%	+
	11	83.71%	0.29%	83.59%	0.31%	+	83.27%	0.35%	+	81.53%	0.54%	+	81.85%	0.54%	+
	12	84.39%	0.36%	84.13%	0.35%	+	84.06%	0.42%	+	81.81%	0.47%	+	81.84%	0.36%	+
	13	84.10%	0.31%	84.01%	0.35%	=	83.65%	0.44%	+	81.90%	0.39%	+	81.82%	0.40%	+
	W/T/L	–/–/–		11/2/0			13/0/0			11/0/2			11/0/2		
Total	W/T/L	–/–/–		23/16/0			39/0/0			33/1/5			33/1/5		

Table 9 and Table 10 present the numerical and statistical test results of the corresponding 51 independent experiments.

From Table 9, it can be seen that when the number of turbines is 15, 20, and 25, HGPSO is significantly better than AGPSO in 1, 8, and 9 problems, respectively, totaling 18 problems, shows comparable performance to AGPSO in 15 problems, and performs worse in one problem. Compared to GLPSO, SUGGA, and AGA, HGPSO achieves total W/T/L results of 36/3/0, 34/4/1, and 39/0/0, respectively.

The results in Table 10 show that compared to CGA, SHADE, IMODE, and SSM, HGPSO is significantly better in all 39 WFLOPs. These results indicate that in wind scenario 3, HGPSO's performance still significantly surpasses that of other competitors and successfully advances the adaptability of PSO variants to WFLOP.

4.5 Statistical results under the wind scenario 4

To further validate the performance of HGPSO under more complex wind scenarios, wind scenario 4 employs a scenario of 12 wind directions and 3 wind speeds, with specific parameter values shown in Table 3. Table 11 and Table 12 present the numerical and statistical test results of the corresponding 51 independent experiments.

From Table 11, it can be seen that when the number of

Table 8 The comparison results of HGPSO and other competitors in wind scenario 2 in solving WFLOP under turbine number of 15, 20, and 25.

Turbine	Problem	HGPSO		CGA			SHADE			IMODE			SSM		
		Mean	SD	Mean	SD	W	Mean	SD	W	Mean	SD	W	Mean	SD	W
15	1	97.09%	0.23%	93.98%	0.57%	+	96.45%	0.34%	+	96.52%	0.26%	+	92.11%	0.80%	+
	2	95.00%	0.34%	92.84%	0.82%	+	94.32%	0.34%	+	94.43%	0.40%	+	89.86%	0.80%	+
	3	95.65%	0.21%	93.07%	0.63%	+	95.26%	0.25%	+	95.19%	0.26%	+	91.08%	0.63%	+
	4	94.95%	0.35%	92.64%	0.96%	+	94.28%	0.48%	+	94.50%	0.33%	+	89.85%	0.71%	+
	5	95.60%	0.24%	93.16%	0.64%	+	95.08%	0.35%	+	95.15%	0.33%	+	90.94%	0.82%	+
	6	96.56%	0.33%	93.16%	0.54%	+	95.79%	0.47%	+	95.93%	0.37%	+	91.53%	0.67%	+
	7	96.69%	0.23%	93.67%	0.53%	+	96.25%	0.42%	+	96.27%	0.24%	+	91.01%	1.04%	+
	8	96.13%	0.31%	93.57%	0.85%	+	95.60%	0.41%	+	95.60%	0.28%	+	91.01%	0.78%	+
	9	96.49%	0.21%	93.51%	0.60%	+	95.85%	0.40%	+	95.98%	0.29%	+	91.58%	0.71%	+
	10	96.20%	0.26%	93.29%	0.86%	+	95.49%	0.58%	+	95.67%	0.25%	+	90.80%	0.81%	+
	11	96.42%	0.25%	93.53%	0.54%	+	95.97%	0.34%	+	95.96%	0.30%	+	91.46%	0.75%	+
	12	97.02%	0.27%	93.79%	0.60%	+	96.30%	0.40%	+	96.29%	0.31%	+	92.12%	0.85%	+
	13	96.83%	0.16%	93.70%	0.65%	+	96.30%	0.42%	+	96.31%	0.25%	+	91.51%	0.92%	+
	W/T/L	–/–/–		13/0/0			13/0/0			13/0/0			13/0/0		
Turbine	Problem	HGPSO		CGA			SHADE			IMODE			SSM		
		Mean	SD	Mean	SD	W	Mean	SD	W	Mean	SD	W	Mean	SD	W
20	1	91.48%	0.39%	86.83%	0.68%	+	89.69%	0.58%	+	89.28%	0.49%	+	84.33%	0.67%	+
	2	87.52%	0.30%	84.92%	0.85%	+	86.04%	0.65%	+	85.61%	0.46%	+	80.84%	0.58%	+
	3	89.42%	0.24%	85.48%	0.84%	+	88.34%	0.42%	+	87.63%	0.52%	+	82.85%	0.64%	+
	4	87.56%	0.30%	84.58%	1.20%	+	86.26%	0.59%	+	85.70%	0.46%	+	80.96%	0.77%	+
	5	89.41%	0.23%	85.49%	0.76%	+	88.01%	0.61%	+	87.64%	0.45%	+	82.76%	0.63%	+
	6	89.87%	0.24%	85.96%	0.64%	+	88.78%	0.55%	+	88.22%	0.36%	+	83.83%	0.60%	+
	7	89.95%	0.38%	85.86%	0.75%	+	88.29%	0.72%	+	88.05%	0.49%	+	82.68%	0.83%	+
	8	89.72%	0.36%	85.88%	0.91%	+	87.90%	0.47%	+	87.58%	0.48%	+	82.74%	0.78%	+
	9	90.60%	0.36%	86.21%	0.67%	+	89.08%	0.73%	+	88.62%	0.51%	+	83.77%	0.73%	+
	10	89.68%	0.34%	85.60%	1.01%	+	87.97%	0.70%	+	87.69%	0.44%	+	83.04%	0.70%	+
	11	90.50%	0.39%	86.28%	0.66%	+	89.03%	0.69%	+	88.63%	0.51%	+	83.66%	0.72%	+
	12	90.83%	0.33%	86.53%	0.58%	+	89.57%	0.52%	+	88.95%	0.40%	+	84.43%	0.75%	+
	13	90.84%	0.39%	86.47%	0.66%	+	89.06%	0.56%	+	88.87%	0.39%	+	83.48%	0.83%	+
	W/T/L	–/–/–		13/0/0			13/0/0			13/0/0			13/0/0		
Turbine	Problem	HGPSO		CGA			SHADE			IMODE			SSM		
		Mean	SD	Mean	SD	W	Mean	SD	W	Mean	SD	W	Mean	SD	W
25	1	84.74%	0.24%	79.73%	0.47%	+	82.59%	0.54%	+	81.37%	0.53%	+	77.22%	0.54%	+
	2	79.81%	0.27%	77.42%	1.10%	+	77.88%	0.53%	+	77.07%	0.46%	+	73.09%	0.58%	+
	3	82.36%	0.36%	78.48%	0.96%	+	80.51%	0.69%	+	79.38%	0.49%	+	75.66%	0.64%	+
	4	79.78%	0.28%	77.15%	1.41%	+	77.87%	0.87%	+	77.07%	0.43%	+	73.16%	0.54%	+
	5	82.39%	0.28%	78.55%	0.87%	+	80.45%	0.80%	+	79.37%	0.47%	+	75.45%	0.61%	+
	6	83.49%	0.30%	79.06%	0.69%	+	81.95%	0.47%	+	80.73%	0.53%	+	76.95%	0.56%	+
	7	83.06%	0.37%	78.28%	0.53%	+	80.65%	0.67%	+	79.60%	0.56%	+	74.78%	0.70%	+
	8	82.38%	0.30%	78.62%	0.78%	+	80.42%	0.59%	+	79.37%	0.45%	+	75.44%	0.65%	+
	9	83.63%	0.30%	79.09%	0.63%	+	81.61%	0.67%	+	80.53%	0.56%	+	76.61%	0.70%	+
	10	82.39%	0.33%	78.57%	0.78%	+	80.57%	0.57%	+	79.52%	0.50%	+	75.46%	0.61%	+
	11	83.71%	0.29%	79.05%	0.63%	+	81.32%	0.78%	+	80.60%	0.52%	+	76.57%	0.54%	+
	12	84.39%	0.36%	79.71%	0.63%	+	82.41%	0.63%	+	81.36%	0.61%	+	77.25%	0.43%	+
	13	84.10%	0.31%	79.41%	0.57%	+	81.67%	0.79%	+	80.81%	0.51%	+	76.30%	0.80%	+
	W/T/L	–/–/–		13/0/0			13/0/0			13/0/0			13/0/0		
Total	W/T/L	–/–/–		39/0/0			39/0/0			39/0/0			39/0/0		

turbines is 15, 20, and 25, HGPSO is significantly better than AGPSO in 4, 10, and 11 problems, respectively, totaling 25 problems, and shows comparable performance to AGPSO in the other 14 problems. This indicates that the proposed level-direction guided hierarchical PSO operator is more effective in highly complex wind scenarios, as HGPSO demonstrates superiority in significantly more wind scenario subproblems without any performance degradation. Additionally, compared to GLPSO, SUGGA, and AGA, HGPSO achieves a perfect win record of 39/0/0 in each comparison.

The results in Table 12 show that HGPSO also achieves a 39/0/0 result against CGA, SHADE, IMODE, and SSM. Moreover, HGPSO exhibits more pronounced superiority at higher turbine dimensions than in the simpler wind scenarios. These results indicate that, in the most complex wind scenario 4, the relative advantage of HGPSO becomes clearer as the problem dimension increases. In this setting, the method remains strongly competitive both against WFLOP-specific baselines and against the tested general-purpose metaheuristics.

Fig. 19 shows the average convergence process of all tested algorithms in solving three WFLOPs (with turbine numbers $N = 15, 20, 25$ and constraint types $C = 10, 1, 8$) over 51 independent optimizations. From Fig. 19, it can be seen

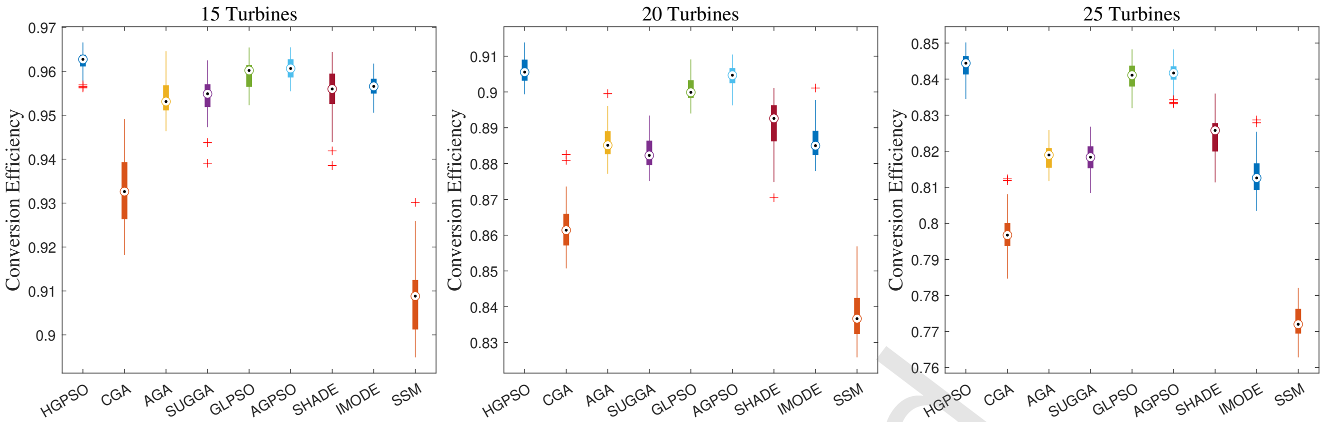

Fig. 14 The boxplot of HGPSO compared with other competitors in wind scenario 2.

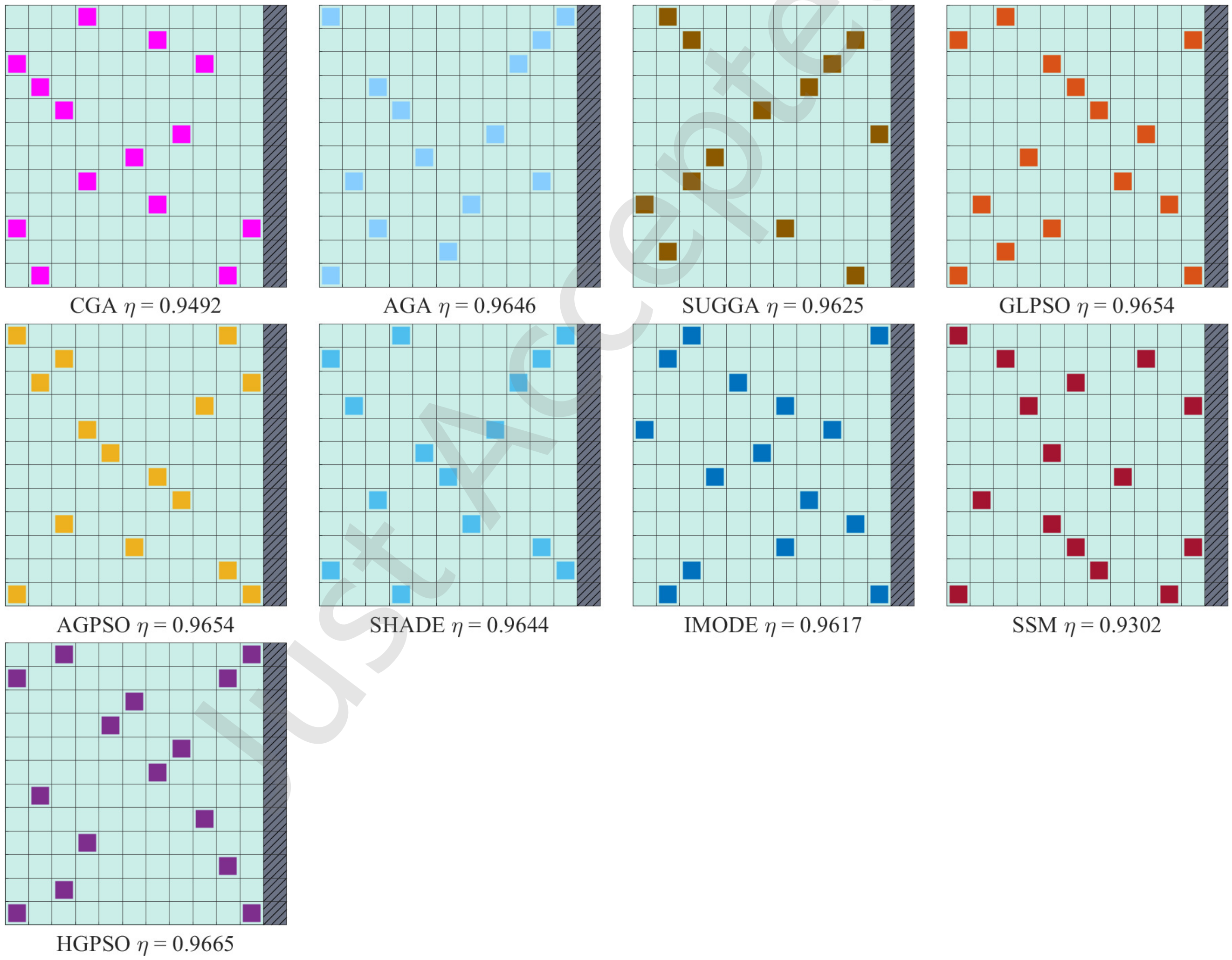

Fig. 15 The visualization of WFLOP solutions obtained from HGPSO and other competitors in wind scenario 2.

that HGPSO's convergence speed remains among the fastest. As the turbine dimension increases, HGPSO's convergence speed becomes even quicker, widening the performance and convergence speed gap with other algorithms.

Fig. 20 shows the box plot graphs. HGPSO not only attains the best average performance, but also exhibits a comparatively concentrated distribution. In addition, several runs reach solutions that are slightly better than the central trend of the box would suggest. This pattern indicates that HGPSO is

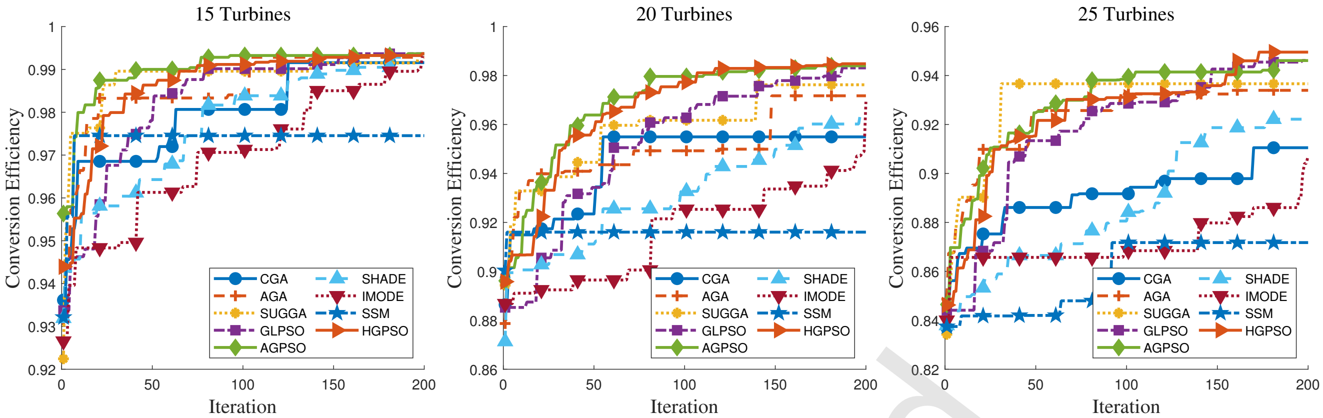

Fig. 16 The convergence plot of HGPSO compared with other competitors in wind scenario 3.

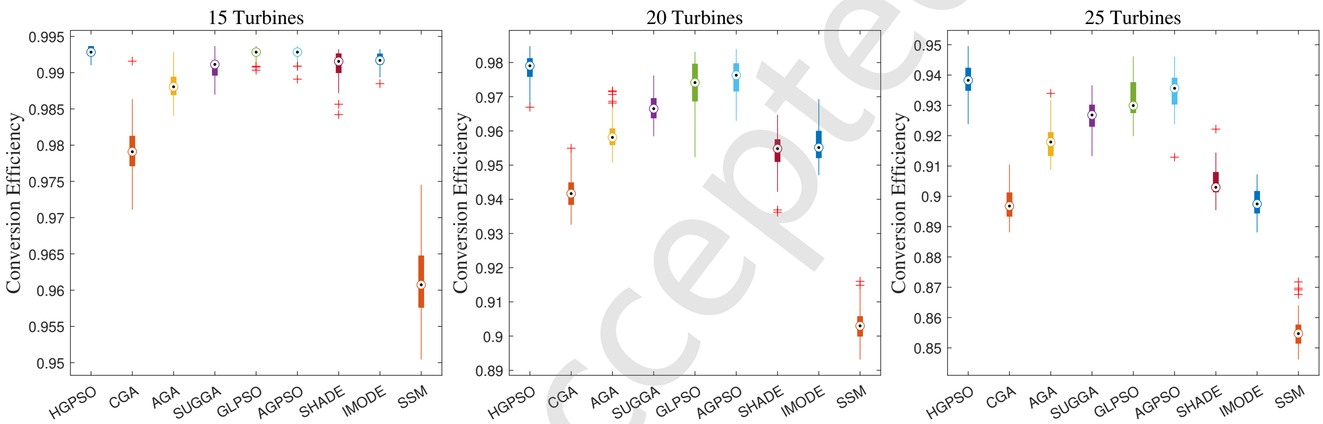

Fig. 17 The boxplot of HGPSO compared with other competitors in wind scenario 3.

strong on average while also maintaining favorable robustness in high-dimensional and complex wind scenarios.

Fig. 21 shows a WFLOP example with 25 turbines under Constraint 8. While the results in Fig. 12, Fig. 15, and Fig. 18 are already evident, Fig. 21 further shows that HGPSO layout appears relatively organized in this example and is associated with higher conversion efficiency than those of the competitors. This visual evidence suggests that the hierarchical guidance mechanism can improve both energy capture and layout regularity in difficult WFLOP instances.

5 Conclusion

Building on AGPSO, this study proposed a level-direction guided hierarchical PSO operator for WFLOP and evaluated it on 156 benchmark instances spanning 4 wind scenarios, 13 land-use conditions, and 3 turbine numbers. Across these tests, HGPSO showed consistently strong convergence behavior, robustness, and statistical competitiveness relative to 5 WFLOP-specific baselines and 3 high-performing general-purpose metaheuristics. The advantage was particularly clear in more constrained and higher-dimensional settings, where the hierarchical guidance mechanism appears to use the fixed FE budget more effectively. In addition to the statistical improvements, representative layout visualizations show that HGPSO can produce feasible layouts with relatively organized spatial patterns in several constrained cases, which may be beneficial for installation planning, maintenance access, and practical land-use organization.

At the same time, the present evidence should be interpreted within clear boundaries. First, HGPSO is still influenced by parameter settings such as m, r_w, and the population size; the appendix therefore provides targeted representative sensitivity evidence rather than claiming exhaustive tuning over all 156 scenarios. Second, the hierarchical guidance mechanism introduces additional optimizer-side overhead, while the total runtime remains dominated by wake evaluation. Since all algorithms are compared under the same maximum function-evaluation budget, the reported performance gains are mainly attributed to more effective use of the available evaluations rather than to additional objective-function calls. Therefore, the improvement of HGPSO should be interpreted together with this limited extra update cost. Third, the current validation is based on grid-based WFLOP benchmarks.

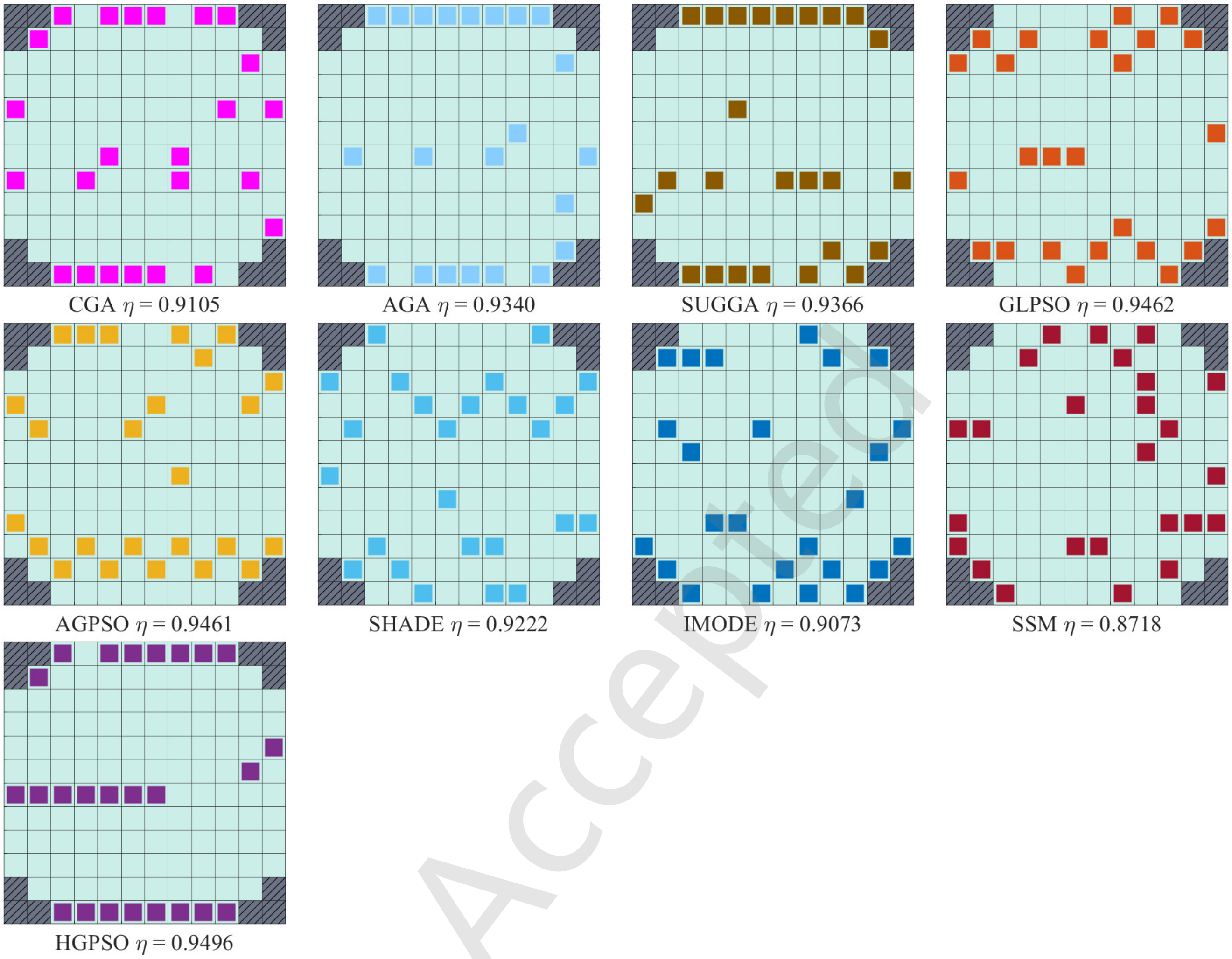

Fig. 18 The visualization of WFLOP solutions obtained from HGPSO and other competitors in wind scenario 3.

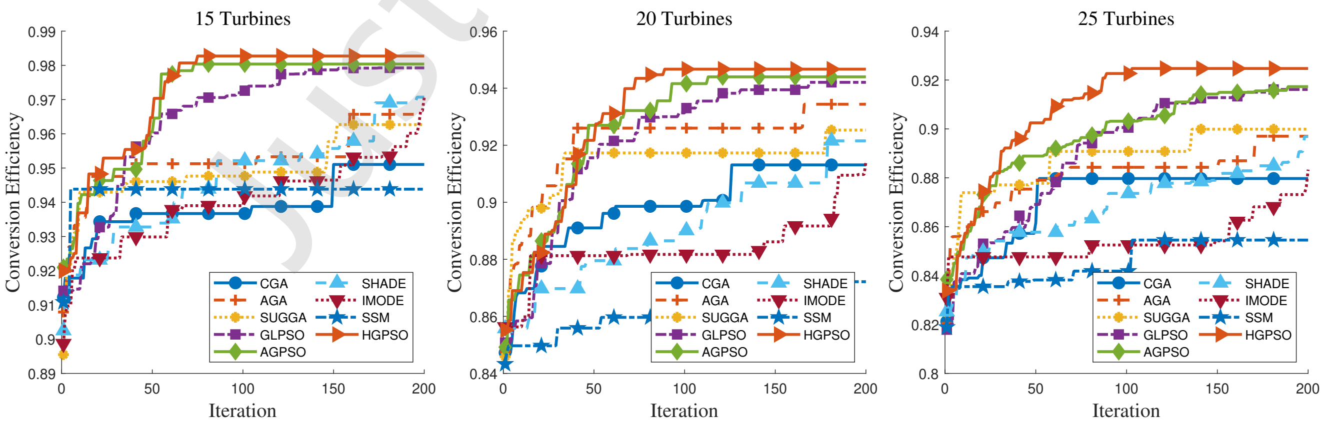

Fig. 19 The convergence plot of HGPSO compared with other competitors in wind scenario 4.

Although this setting enables fair comparison with existing benchmark algorithms and simplifies feasibility control, it may introduce discretization effects because turbine positions are restricted to predefined grid-cell centers. In addition, these benchmark cases do not explicitly model real-world terrain variability, such as elevation changes, irregular ground surfaces, or spatially varying roughness, and the wind conditions are represented by predefined probability settings rather than stochastic uncertainty models derived from measured wind data. Therefore, the obtained layouts should be interpreted as

Table 9 The comparison results of HGPSO and other competitors in wind scenario 3 in solving WFLOP under turbine number of 15, 20, and 25.

Turbine	Problem	HGPSO		AGPSO			GLPSO			SUGGA			AGA		
		Mean	SD	Mean	SD	W	Mean	SD	W	Mean	SD	W	Mean	SD	W
15	1	99.27%	0.10%	99.25%	0.10%	=	99.15%	0.21%	+	99.03%	0.18%	+	98.64%	0.25%	+
	2	98.82%	0.23%	98.91%	0.17%	-	98.80%	0.25%	=	98.58%	0.22%	+	98.30%	0.33%	+
	3	99.28%	0.08%	99.26%	0.09%	=	99.24%	0.10%	+	99.08%	0.14%	+	98.79%	0.20%	+
	4	98.74%	0.14%	98.72%	0.15%	=	98.58%	0.24%	+	99.01%	0.20%	-	98.36%	0.41%	+
	5	98.72%	0.15%	98.71%	0.17%	=	98.63%	0.19%	+	98.63%	0.30%	+	98.28%	0.29%	+
	6	99.30%	0.07%	99.27%	0.09%	=	99.27%	0.08%	=	99.08%	0.16%	+	98.81%	0.21%	+
	7	99.03%	0.25%	98.94%	0.27%	+	98.86%	0.29%	+	98.57%	0.25%	+	98.09%	0.29%	+
	8	99.10%	0.12%	99.08%	0.14%	=	99.07%	0.15%	=	98.80%	0.24%	+	98.56%	0.24%	+
	9	99.26%	0.11%	99.27%	0.10%	=	99.21%	0.13%	+	99.02%	0.15%	+	98.82%	0.24%	+
	10	98.98%	0.13%	99.00%	0.11%	=	98.93%	0.18%	+	99.02%	0.24%	=	98.57%	0.34%	+
	11	98.99%	0.13%	99.01%	0.10%	=	98.90%	0.19%	+	98.88%	0.23%	+	98.41%	0.24%	+
	12	99.26%	0.11%	99.26%	0.08%	=	99.21%	0.14%	+	99.04%	0.15%	+	98.74%	0.24%	+
	13	99.09%	0.19%	99.09%	0.17%	=	98.94%	0.27%	+	98.54%	0.29%	+	98.19%	0.36%	+
	W/T/L	–/–/–		1/11/1			10/3/0			11/1/1			13/0/0		
Turbine	Problem	HGPSO		AGPSO			GLPSO			SUGGA			AGA		
		Mean	SD	Mean	SD	W	Mean	SD	W	Mean	SD	W	Mean	SD	W
20	1	98.08%	0.45%	97.85%	0.42%	+	97.50%	0.61%	+	97.17%	0.37%	+	96.23%	0.46%	+
	2	97.41%	0.59%	97.36%	0.55%	=	97.14%	0.53%	+	96.03%	0.52%	+	95.49%	0.54%	+
	3	98.21%	0.35%	97.98%	0.38%	+	97.85%	0.48%	+	97.25%	0.34%	+	96.58%	0.42%	+
	4	96.98%	0.53%	96.81%	0.68%	=	96.60%	0.61%	+	96.87%	0.48%	=	95.70%	0.52%	+
	5	97.49%	0.43%	97.04%	0.57%	+	96.74%	0.47%	+	96.16%	0.47%	+	95.54%	0.50%	+
	6	98.32%	0.29%	98.26%	0.33%	=	98.00%	0.45%	+	97.30%	0.39%	+	96.53%	0.40%	+
	7	96.76%	0.48%	96.72%	0.58%	=	96.37%	0.63%	+	96.21%	0.34%	+	95.31%	0.53%	+
	8	97.82%	0.44%	97.53%	0.55%	+	97.30%	0.75%	+	96.69%	0.42%	+	95.89%	0.53%	+
	9	98.16%	0.43%	98.05%	0.41%	=	97.87%	0.45%	+	97.17%	0.37%	+	96.56%	0.40%	+
	10	97.81%	0.47%	97.43%	0.57%	+	97.20%	0.58%	+	97.03%	0.47%	+	96.05%	0.36%	+
	11	97.89%	0.35%	97.46%	0.49%	+	97.26%	0.55%	+	96.69%	0.44%	+	96.01%	0.47%	+
	12	98.24%	0.36%	98.03%	0.39%	+	97.75%	0.36%	+	97.25%	0.38%	+	96.48%	0.40%	+
	13	97.22%	0.44%	97.04%	0.53%	+	96.72%	0.45%	+	95.91%	0.51%	+	95.14%	0.51%	+
	W/T/L	–/–/–		8/5/0			13/0/0			12/1/0			13/0/0		
Turbine	Problem	HGPSO		AGPSO			GLPSO			SUGGA			AGA		
		Mean	SD	Mean	SD	W	Mean	SD	W	Mean	SD	W	Mean	SD	W
25	1	95.92%	0.76%	95.71%	0.81%	=	95.11%	0.79%	+	94.59%	0.42%	+	93.65%	0.55%	+
	2	94.91%	0.92%	94.39%	0.72%	+	93.84%	0.81%	+	92.67%	0.48%	+	92.33%	0.58%	+
	3	95.65%	0.74%	95.48%	0.85%	=	95.03%	0.68%	+	94.69%	0.35%	+	93.77%	0.38%	+
	4	94.20%	0.88%	93.96%	0.81%	=	93.15%	0.94%	+	94.10%	0.67%	=	92.60%	0.73%	+
	5	94.14%	0.46%	93.71%	0.60%	+	93.43%	0.60%	+	93.19%	0.60%	+	92.49%	0.64%	+
	6	95.83%	0.91%	95.47%	0.82%	+	95.28%	0.83%	+	94.66%	0.56%	+	93.86%	0.41%	+
	7	93.42%	0.74%	93.13%	0.62%	+	93.01%	0.54%	+	93.29%	0.55%	=	92.25%	0.69%	+
	8	95.60%	0.83%	95.18%	0.92%	+	94.58%	0.71%	+	93.83%	0.47%	+	93.12%	0.62%	+
	9	95.93%	0.73%	95.66%	0.73%	+	95.08%	0.73%	+	94.67%	0.54%	+	93.79%	0.54%	+
	10	95.35%	0.69%	94.77%	0.85%	+	94.22%	0.79%	+	94.37%	0.57%	+	93.22%	0.60%	+
	11	94.85%	0.73%	94.87%	0.73%	=	94.19%	0.69%	+	93.93%	0.59%	+	93.18%	0.65%	+
	12	95.97%	0.85%	95.52%	0.89%	+	95.15%	0.79%	+	94.63%	0.36%	+	93.87%	0.53%	+
	13	93.85%	0.54%	93.47%	0.60%	+	93.21%	0.73%	+	92.66%	0.58%	+	91.79%	0.56%	+
	W/T/L	–/–/–		9/4/0			13/0/0			11/2/0			13/0/0		
Total	W/T/L	–/–/–		18/20/1			36/3/0			34/4/1			39/0/0		

optimized solutions within the adopted benchmark framework rather than direct site-specific wind farm designs. Future work may consider finer-resolution grids, continuous-coordinate extensions, larger-scale benchmark cases, and more realistic benchmark settings involving terrain-related factors and measured wind distributions.

A Technical appendix on parameter sensitivity and algorithmic properties

A.1 Representative parameter sensitivity study

To complement the main experiments, we conducted a representative one-factor-at-a-time sensitivity study on two benchmark instances under the same FE budget used throughout the paper ($maxFEs = 24000$). Because each sensitivity run retains the same wake-evaluation cost as a main benchmark run, we chose a targeted representative appendix study rather than an exhaustive sweep over all 156 benchmark instances. Case A is a medium-difficulty benchmark instance under wind scenario WS2 on a 12×12 wind farm with $N = 20$ turbines and land-use constraint type 9. Case B is a higher-dimensional and more constrained benchmark instance under wind scenario WS3 on a 12×12 wind farm with $N = 25$ turbines and land-use constraint type 12. The baseline HGPSO parameters are $NP = 120$, $c = 1.49618$, $p_m = 0.01$, $m = 0.9$,

Table 10 The comparison results of HGPSO and other competitors in wind scenario 3 in solving WFLOP under turbine number of 15, 20, and 25.

Turbine	Problem	HGPSO		CGA			SHADE			IMODE			SSM		
		Mean	SD	Mean	SD	W	Mean	SD	W	Mean	SD	W	Mean	SD	W
15	1	99.27%	0.10%	97.85%	0.38%	+	98.88%	0.25%	+	99.10%	0.15%	+	95.61%	0.58%	+
	2	98.82%	0.23%	97.22%	0.44%	+	98.44%	0.25%	+	98.75%	0.20%	+	94.71%	0.63%	+
	3	99.28%	0.08%	97.98%	0.37%	+	99.14%	0.19%	+	99.19%	0.11%	+	96.27%	0.42%	+
	4	98.74%	0.14%	97.15%	0.48%	+	98.16%	0.25%	+	98.47%	0.20%	+	94.21%	0.49%	+
	5	98.72%	0.15%	97.20%	0.45%	+	98.22%	0.26%	+	98.48%	0.19%	+	94.89%	0.53%	+
	6	99.30%	0.07%	97.94%	0.39%	+	99.11%	0.19%	+	99.17%	0.11%	+	96.07%	0.52%	+
	7	99.03%	0.25%	97.02%	0.36%	+	98.15%	0.36%	+	98.57%	0.25%	+	94.41%	0.59%	+
	8	99.10%	0.12%	97.55%	0.54%	+	98.60%	0.33%	+	98.95%	0.17%	+	94.88%	0.57%	+
	9	99.26%	0.11%	97.89%	0.35%	+	99.05%	0.20%	+	99.17%	0.12%	+	95.79%	0.48%	+
	10	98.98%	0.13%	97.52%	0.38%	+	98.52%	0.33%	+	98.81%	0.17%	+	94.97%	0.70%	+
	11	98.99%	0.13%	97.45%	0.43%	+	98.55%	0.23%	+	98.85%	0.17%	+	95.12%	0.52%	+
	12	99.26%	0.11%	97.90%	0.29%	+	99.04%	0.29%	+	99.17%	0.12%	+	95.77%	0.58%	+
	13	99.09%	0.19%	97.30%	0.40%	+	98.44%	0.30%	+	98.70%	0.25%	+	94.66%	0.51%	+
	W/T/L	–/–/–		13/0/0			13/0/0			13/0/0			13/0/0		
Turbine	Problem	HGPSO		CGA			SHADE			IMODE			SSM		
		Mean	SD	Mean	SD	W	Mean	SD	W	Mean	SD	W	Mean	SD	W
20	1	98.08%	0.45%	94.61%	0.57%	+	95.93%	0.35%	+	95.87%	0.41%	+	90.89%	0.55%	+
	2	97.41%	0.59%	93.63%	0.53%	+	94.86%	0.55%	+	94.97%	0.49%	+	89.37%	0.50%	+
	3	98.21%	0.35%	94.94%	0.49%	+	96.58%	0.42%	+	96.21%	0.41%	+	92.16%	0.61%	+
	4	96.98%	0.53%	93.65%	0.77%	+	94.51%	0.65%	+	94.60%	0.58%	+	89.43%	0.62%	+
	5	97.49%	0.43%	93.82%	0.59%	+	94.89%	0.45%	+	94.82%	0.40%	+	90.45%	0.53%	+
	6	98.32%	0.29%	94.89%	0.61%	+	96.42%	0.57%	+	96.16%	0.33%	+	91.91%	0.57%	+
	7	96.76%	0.48%	93.38%	0.53%	+	94.33%	0.53%	+	94.38%	0.36%	+	89.29%	0.48%	+
	8	97.82%	0.44%	94.20%	0.53%	+	95.42%	0.60%	+	95.58%	0.52%	+	90.38%	0.56%	+
	9	98.16%	0.43%	94.91%	0.50%	+	96.31%	0.69%	+	95.98%	0.41%	+	91.64%	0.54%	+
	10	97.81%	0.47%	94.02%	0.50%	+	95.30%	0.54%	+	95.22%	0.36%	+	90.26%	0.67%	+
	11	97.89%	0.35%	94.26%	0.51%	+	95.46%	0.41%	+	95.31%	0.47%	+	90.68%	0.60%	+
	12	98.24%	0.36%	94.77%	0.51%	+	96.34%	0.52%	+	96.05%	0.46%	+	91.73%	0.73%	+
	13	97.22%	0.44%	93.60%	0.48%	+	94.81%	0.41%	+	94.75%	0.44%	+	89.90%	0.52%	+
	W/T/L	–/–/–		13/0/0			13/0/0			13/0/0			13/0/0		
Turbine	Problem	HGPSO		CGA			SHADE			IMODE			SSM		
		Mean	SD	Mean	SD	W	Mean	SD	W	Mean	SD	W	Mean	SD	W
25	1	95.92%	0.76%	91.44%	0.55%	+	92.19%	0.49%	+	91.38%	0.51%	+	86.92%	0.66%	+
	2	94.91%	0.92%	90.01%	0.81%	+	90.72%	0.67%	+	89.68%	0.59%	+	85.13%	0.57%	+
	3	95.65%	0.74%	91.87%	0.68%	+	92.78%	0.75%	+	91.80%	0.46%	+	88.16%	0.64%	+
	4	94.20%	0.88%	90.15%	0.73%	+	90.43%	0.59%	+	89.38%	0.41%	+	84.83%	0.68%	+
	5	94.14%	0.46%	90.20%	0.56%	+	91.05%	0.56%	+	90.33%	0.47%	+	86.38%	0.57%	+
	6	95.83%	0.91%	91.54%	0.56%	+	92.79%	0.57%	+	91.75%	0.57%	+	87.92%	0.57%	+
	7	93.42%	0.74%	89.78%	0.58%	+	90.20%	0.62%	+	89.47%	0.48%	+	84.88%	0.60%	+
	8	95.60%	0.83%	90.55%	0.58%	+	91.28%	0.76%	+	90.52%	0.45%	+	86.00%	0.59%	+
	9	95.93%	0.73%	91.57%	0.56%	+	92.59%	0.60%	+	91.65%	0.53%	+	87.43%	0.45%	+
	10	95.35%	0.69%	90.64%	0.64%	+	91.38%	0.75%	+	90.48%	0.60%	+	85.84%	0.53%	+
	11	94.85%	0.73%	90.93%	0.65%	+	91.59%	0.53%	+	90.78%	0.52%	+	86.65%	0.59%	+
	12	95.97%	0.85%	91.55%	0.65%	+	92.58%	0.68%	+	91.63%	0.50%	+	87.54%	0.63%	+
	13	93.85%	0.54%	89.73%	0.50%	+	90.47%	0.50%	+	89.81%	0.46%	+	85.56%	0.57%	+
	W/T/L	–/–/–		13/0/0			13/0/0			13/0/0			13/0/0		
Total	W/T/L	–/–/–		39/0/0			39/0/0			39/0/0			39/0/0		

and $r_w = 0.1$. For each parameter value in each case, three independent runs were executed. The results are summarized in Table 13.

As shown in Table 13, the results for m, r_w, and NP indicate that HGPSO is not overly sensitive to moderate parameter changes in the two representative cases. For the branch threshold, $m = 0.90$ provides stable performance and avoids the larger fluctuation observed when $m = 0.95$ in Case B. For the replacement-pool ratio, $r_w = 0.10$ achieves a stable balance between exploiting high-quality candidate positions and maintaining search diversity. For the population size, the performance differences among $NP = 80$, $NP = 120$, and $NP = 160$ are moderate. Therefore, $NP = 120$ is retained as the default setting because it provides competitive performance while remaining consistent with the benchmark setting used in the main experiments. Overall, the default configuration $m = 0.90$, $r_w = 0.10$, and $NP = 120$ provides a reasonable and stable parameter setting in the tested representative cases.

Several observations can be made from Table 13. First, in Case A, the default settings used in the main experiments generally show competitive mean performance and stable behavior among the tested parameter values. Second, in the more demanding Case B, nearby parameter values sometimes

Table 11 The comparison results of HGPSO and other competitors in wind scenario 4 in solving WFLOP under turbine number of 15, 20, and 25.

Turbine	Problem	HGPSO		AGPSO			GLPSO			SUGGA			AGA		
		Mean	SD	Mean	SD	W	Mean	SD	W	Mean	SD	W	Mean	SD	W
15	1	97.64%	0.39%	97.51%	0.37%	=	97.16%	0.39%	+	95.54%	0.35%	+	95.47%	0.32%	+
	2	96.83%	0.66%	96.69%	0.72%	=	96.34%	0.66%	+	95.32%	0.44%	+	95.28%	0.52%	+
	3	97.21%	0.30%	97.09%	0.28%	+	96.91%	0.33%	+	95.46%	0.31%	+	95.45%	0.25%	+
	4	96.65%	0.70%	96.47%	0.70%	=	96.29%	0.52%	+	95.58%	0.39%	+	95.25%	0.44%	+
	5	97.10%	0.33%	97.03%	0.27%	+	96.96%	0.28%	+	95.57%	0.29%	+	95.49%	0.34%	+
	6	97.09%	0.32%	96.95%	0.27%	+	96.90%	0.33%	+	95.43%	0.28%	+	95.35%	0.26%	+
	7	97.01%	0.52%	96.96%	0.53%	=	96.74%	0.51%	+	95.45%	0.32%	+	95.22%	0.35%	+
	8	97.24%	0.58%	97.09%	0.46%	=	96.89%	0.51%	+	95.60%	0.28%	+	95.51%	0.39%	+
	9	97.28%	0.35%	97.21%	0.32%	=	97.02%	0.35%	+	95.48%	0.27%	+	95.35%	0.31%	+
	10	97.25%	0.60%	97.06%	0.44%	=	96.66%	0.39%	+	95.43%	0.39%	+	95.39%	0.40%	+
	11	97.36%	0.35%	97.21%	0.28%	+	97.14%	0.32%	+	95.52%	0.34%	+	95.51%	0.38%	+
	12	97.24%	0.28%	97.14%	0.33%	=	97.03%	0.33%	+	95.37%	0.25%	+	95.45%	0.35%	+
	13	97.37%	0.42%	97.35%	0.45%	=	97.00%	0.50%	+	95.64%	0.28%	+	95.47%	0.39%	+
	W/T/L	–/–/–		4/9/0			13/0/0			13/0/0			13/0/0		
Turbine	Problem	HGPSO		AGPSO			GLPSO			SUGGA			AGA		
		Mean	SD	Mean	SD	W	Mean	SD	W	Mean	SD	W	Mean	SD	W
20	1	94.63%	0.60%	94.66%	0.74%	=	94.29%	0.43%	+	92.05%	0.40%	+	91.96%	0.38%	+
	2	93.25%	0.61%	92.94%	0.53%	+	92.49%	0.47%	+	91.55%	0.42%	+	91.45%	0.61%	+
	3	94.23%	0.37%	94.23%	0.32%	=	94.01%	0.41%	+	92.05%	0.34%	+	92.05%	0.37%	+
	4	93.06%	0.54%	92.79%	0.56%	+	92.75%	0.55%	+	91.76%	0.51%	+	91.60%	0.49%	+
	5	94.28%	0.39%	94.10%	0.31%	+	93.97%	0.40%	+	92.06%	0.37%	+	92.03%	0.35%	+
	6	94.30%	0.29%	94.03%	0.32%	+	93.86%	0.35%	+	92.05%	0.37%	+	92.13%	0.38%	+
	7	93.91%	0.60%	93.48%	0.56%	+	93.38%	0.54%	+	91.81%	0.42%	+	91.44%	0.45%	+
	8	94.07%	0.69%	93.68%	0.61%	+	93.55%	0.51%	+	92.08%	0.47%	+	91.77%	0.30%	+
	9	94.49%	0.54%	94.29%	0.47%	+	94.17%	0.56%	+	91.99%	0.33%	+	92.05%	0.37%	+
	10	94.04%	0.67%	93.71%	0.57%	+	93.53%	0.56%	+	92.04%	0.38%	+	91.89%	0.44%	+
	11	94.49%	0.47%	94.21%	0.41%	+	94.12%	0.39%	+	92.03%	0.36%	+	92.01%	0.39%	+
	12	94.32%	0.36%	94.14%	0.40%	+	93.89%	0.48%	+	92.04%	0.43%	+	92.00%	0.34%	+
	13	94.27%	0.48%	94.24%	0.63%	=	93.98%	0.58%	+	92.20%	0.43%	+	92.01%	0.27%	+
	W/T/L	–/–/–		10/3/0			13/0/0			13/0/0			13/0/0		
Turbine	Problem	HGPSO		AGPSO			GLPSO			SUGGA			AGA		
		Mean	SD	Mean	SD	W	Mean	SD	W	Mean	SD	W	Mean	SD	W
25	1	91.47%	0.47%	91.20%	0.46%	+	90.79%	0.48%	+	88.71%	0.32%	+	88.72%	0.30%	+
	2	89.25%	0.47%	89.07%	0.45%	+	88.89%	0.45%	+	88.03%	0.46%	+	87.86%	0.55%	+
	3	90.96%	0.37%	90.84%	0.41%	=	90.57%	0.49%	+	88.67%	0.28%	+	88.68%	0.37%	+
	4	89.31%	0.50%	89.07%	0.47%	+	88.86%	0.48%	+	88.28%	0.59%	+	87.78%	0.55%	+
	5	91.06%	0.32%	90.82%	0.26%	+	90.55%	0.48%	+	88.81%	0.33%	+	88.81%	0.28%	+
	6	91.12%	0.38%	90.90%	0.41%	+	90.78%	0.46%	+	88.78%	0.33%	+	88.89%	0.36%	+
	7	90.30%	0.70%	89.78%	0.73%	+	89.35%	0.77%	+	88.14%	0.48%	+	87.75%	0.55%	+
	8	90.48%	0.46%	90.20%	0.48%	+	89.95%	0.49%	+	88.58%	0.48%	+	88.49%	0.35%	+
	9	91.28%	0.36%	90.87%	0.42%	+	90.66%	0.41%	+	88.69%	0.38%	+	88.70%	0.27%	+
	10	90.49%	0.43%	90.15%	0.59%	+	90.02%	0.47%	+	88.61%	0.41%	+	88.46%	0.47%	+
	11	91.16%	0.46%	91.02%	0.41%	+	90.69%	0.44%	+	88.65%	0.30%	+	88.70%	0.36%	+
	12	91.30%	0.35%	90.99%	0.40%	+	90.75%	0.39%	+	88.75%	0.30%	+	88.74%	0.38%	+
	13	90.75%	0.54%	90.62%	0.47%	=	90.39%	0.46%	+	88.86%	0.34%	+	88.48%	0.29%	+
	W/T/L	–/–/–		11/2/0			13/0/0			13/0/0			13/0/0		
Total	W/T/L	–/–/–		25/14/0			39/0/0			39/0/0			39/0/0		

achieve slightly higher mean conversion efficiency, but the default settings remain competitive and avoid large fluctuations in most tested parameter groups. For example, $m = 0.95$ raises the mean slightly relative to $m = 0.90$ in Case B, but also increases the standard deviation from 0.057% to 1.048%. Third, the mutation rate is relatively sensitive in Case A: reducing p_m to 0.005 decreases the mean conversion efficiency by more than one percentage point, whereas increasing it to 0.02 also weakens stability. Fourth, the replacement rule is indeed beneficial, and both cases indicate that a moderate candidate-pool ratio offers good robustness. This also clarifies an imprecise phrase in the original draft: the source implementation does not use a strict fixed top-20% rule for worst-position replacement. Instead, it uses the adaptive pool size $K = \lfloor r_w I_r I_c \rfloor + D$, so the default setting corresponds to $K = 34$ (23.61% of the grid) in Case A and $K = 39$ (27.08% of the grid) in Case B. This adaptive replacement pool should also be distinguished from the separate tournament mechanism, which still uses a fixed 20% random subset after prolonged stagnation. Fifth, the population-size results show that the differences among $NP = 80$, $NP = 120$, and $NP = 160$ are moderate under the same FE budget. Although $NP = 80$ performs better in Case B, $NP = 120$ is retained as the default setting because it provides competitive

Table 12 The comparison results of HGPSO and other competitors in wind scenario 4 in solving WFLOP under turbine number of 15, 20, and 25.

Turbine	Problem	HGPSO		CGA			SHADE			IMODE			SSM		
		Mean	SD	Mean	SD	W	Mean	SD	W	Mean	SD	W	Mean	SD	W
15	1	97.64%	0.39%	94.33%	0.31%	+	96.35%	0.39%	+	96.34%	0.34%	+	92.50%	0.34%	+
	2	96.83%	0.66%	93.60%	0.53%	+	95.26%	0.42%	+	95.27%	0.32%	+	91.31%	0.44%	+
	3	97.21%	0.30%	94.30%	0.44%	+	96.24%	0.29%	+	96.26%	0.34%	+	92.68%	0.38%	+
	4	96.65%	0.70%	93.58%	0.54%	+	95.35%	0.45%	+	95.40%	0.35%	+	91.20%	0.44%	+
	5	97.10%	0.33%	94.34%	0.37%	+	96.19%	0.37%	+	96.25%	0.28%	+	92.68%	0.42%	+
	6	97.09%	0.32%	94.26%	0.34%	+	96.18%	0.29%	+	96.16%	0.26%	+	93.08%	0.46%	+
	7	97.01%	0.52%	93.69%	0.50%	+	95.79%	0.35%	+	95.90%	0.37%	+	91.34%	0.46%	+
	8	97.24%	0.58%	93.97%	0.53%	+	95.88%	0.34%	+	95.79%	0.29%	+	91.92%	0.39%	+
	9	97.28%	0.35%	94.33%	0.38%	+	96.25%	0.32%	+	96.28%	0.31%	+	92.62%	0.38%	+
	10	97.25%	0.60%	94.05%	0.45%	+	95.83%	0.42%	+	95.83%	0.30%	+	92.01%	0.47%	+
	11	97.36%	0.35%	94.35%	0.38%	+	96.31%	0.34%	+	96.28%	0.33%	+	92.66%	0.46%	+
	12	97.24%	0.28%	94.36%	0.39%	+	96.20%	0.30%	+	96.24%	0.33%	+	92.89%	0.39%	+
	13	97.37%	0.42%	94.23%	0.39%	+	95.93%	0.37%	+	96.13%	0.33%	+	92.01%	0.55%	+
	W/T/L	–/–/–		13/0/0			13/0/0			13/0/0			13/0/0		
Turbine	Problem	HGPSO		CGA			SHADE			IMODE			SSM		
		Mean	SD	Mean	SD	W	Mean	SD	W	Mean	SD	W	Mean	SD	W
20	1	94.63%	0.60%	90.38%	0.51%	+	92.36%	0.38%	+	91.88%	0.35%	+	88.12%	0.34%	+
	2	93.25%	0.61%	89.32%	0.63%	+	90.89%	0.48%	+	90.42%	0.37%	+	86.44%	0.36%	+
	3	94.23%	0.37%	90.35%	0.40%	+	92.43%	0.38%	+	91.98%	0.35%	+	88.46%	0.45%	+
	4	93.06%	0.54%	89.26%	0.47%	+	90.82%	0.36%	+	90.49%	0.38%	+	86.48%	0.42%	+
	5	94.28%	0.39%	90.41%	0.44%	+	92.33%	0.36%	+	91.97%	0.38%	+	88.34%	0.48%	+
	6	94.30%	0.29%	90.42%	0.32%	+	92.52%	0.41%	+	92.06%	0.37%	+	88.87%	0.39%	+
	7	93.91%	0.60%	89.27%	0.46%	+	91.11%	0.51%	+	90.83%	0.47%	+	86.44%	0.47%	+
	8	94.07%	0.69%	90.05%	0.45%	+	91.75%	0.44%	+	91.22%	0.49%	+	87.45%	0.45%	+
	9	94.49%	0.54%	90.35%	0.41%	+	92.38%	0.61%	+	91.87%	0.39%	+	88.32%	0.41%	+
	10	94.04%	0.67%	89.81%	0.45%	+	91.61%	0.37%	+	91.19%	0.41%	+	87.42%	0.36%	+
	11	94.49%	0.47%	90.47%	0.46%	+	92.38%	0.37%	+	91.87%	0.35%	+	88.25%	0.39%	+
	12	94.32%	0.36%	90.40%	0.30%	+	92.51%	0.39%	+	91.93%	0.31%	+	88.59%	0.40%	+
	13	94.27%	0.48%	90.26%	0.55%	+	91.84%	0.48%	+	91.51%	0.47%	+	87.40%	0.48%	+
	W/T/L	–/–/–		13/0/0			13/0/0			13/0/0			13/0/0		
Turbine	Problem	HGPSO		CGA			SHADE			IMODE			SSM		
		Mean	SD	Mean	SD	W	Mean	SD	W	Mean	SD	W	Mean	SD	W
25	1	91.47%	0.47%	86.78%	0.49%	+	88.35%	0.43%	+	87.45%	0.39%	+	84.13%	0.37%	+
	2	89.25%	0.47%	85.41%	0.58%	+	86.47%	0.46%	+	85.62%	0.40%	+	82.09%	0.47%	+
	3	90.96%	0.37%	86.64%	0.43%	+	88.65%	0.47%	+	87.40%	0.36%	+	84.36%	0.41%	+
	4	89.31%	0.50%	85.22%	0.51%	+	86.58%	0.37%	+	85.52%	0.31%	+	82.06%	0.44%	+
	5	91.06%	0.32%	86.80%	0.51%	+	88.38%	0.39%	+	87.45%	0.37%	+	84.36%	0.47%	+
	6	91.12%	0.38%	86.84%	0.45%	+	88.61%	0.42%	+	87.72%	0.44%	+	84.82%	0.35%	+
	7	90.30%	0.70%	85.14%	0.48%	+	86.74%	0.47%	+	85.73%	0.34%	+	81.96%	0.43%	+
	8	90.48%	0.46%	86.12%	0.49%	+	87.46%	0.50%	+	86.53%	0.36%	+	83.25%	0.54%	+
	9	91.28%	0.36%	86.68%	0.39%	+	88.61%	0.43%	+	87.37%	0.36%	+	84.24%	0.37%	+
	10	90.49%	0.43%	85.97%	0.42%	+	87.58%	0.46%	+	86.57%	0.37%	+	83.13%	0.48%	+
	11	91.16%	0.46%	86.66%	0.49%	+	88.35%	0.47%	+	87.47%	0.40%	+	84.28%	0.47%	+
	12	91.30%	0.35%	86.81%	0.39%	+	88.67%	0.40%	+	87.57%	0.39%	+	84.59%	0.37%	+
	13	90.75%	0.54%	86.33%	0.45%	+	87.78%	0.41%	+	86.69%	0.44%	+	83.01%	0.43%	+
	W/T/L	–/–/–		13/0/0			13/0/0			13/0/0			13/0/0		
Total	W/T/L	–/–/–		39/0/0			39/0/0			39/0/0			39/0/0		

performance while remaining consistent with the benchmark setting used in the main experiments. Overall, these two representative cases suggest that the adopted defaults, including $m = 0.90$, $r_w = 0.10$, and $NP = 120$, provide a competitive and stable compromise rather than a narrowly tuned choice.

A.2 Complexity discussion

Let k denote the number of outer cycles, NP the population size, $D(= N)$ the number of turbine-index dimensions, $G = I_r I_c$ the number of grid cells, and $S = |\Theta||V|$ the number of wind states used in the wake evaluation. For each cycle, crossover, mutation, hierarchical branching, and tournament-related updates operate on D-dimensional particles, so the optimizer-side update cost is $O(NP \cdot D)$. Feasibility repair and encoding/decoding introduce an additional bookkeeping cost of $O(NP \cdot (D + G))$.

The dominant cost comes from wake evaluation. For each layout and each wind state, the Jensen-style wake computation evaluates pairwise turbine interactions, which scales as $O(D^2)$, while the power aggregation itself is linear in D. Therefore, one full cycle has cost

$$O\Big(NP \cdot (D + G + S\,D^2)\Big), \tag{28}$$

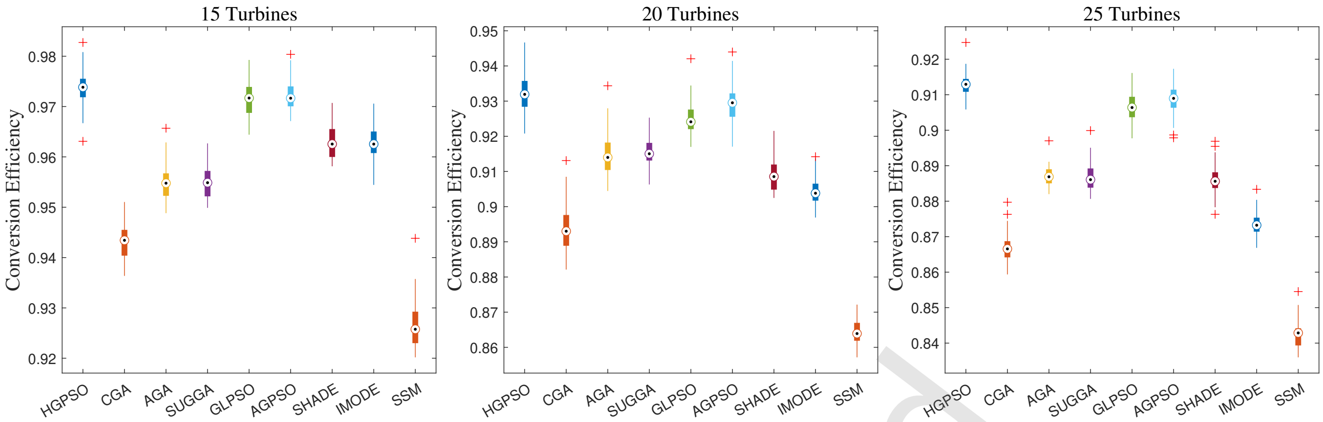

Fig. 20 The boxplot of HGPSO compared with other competitors in wind scenario 4.

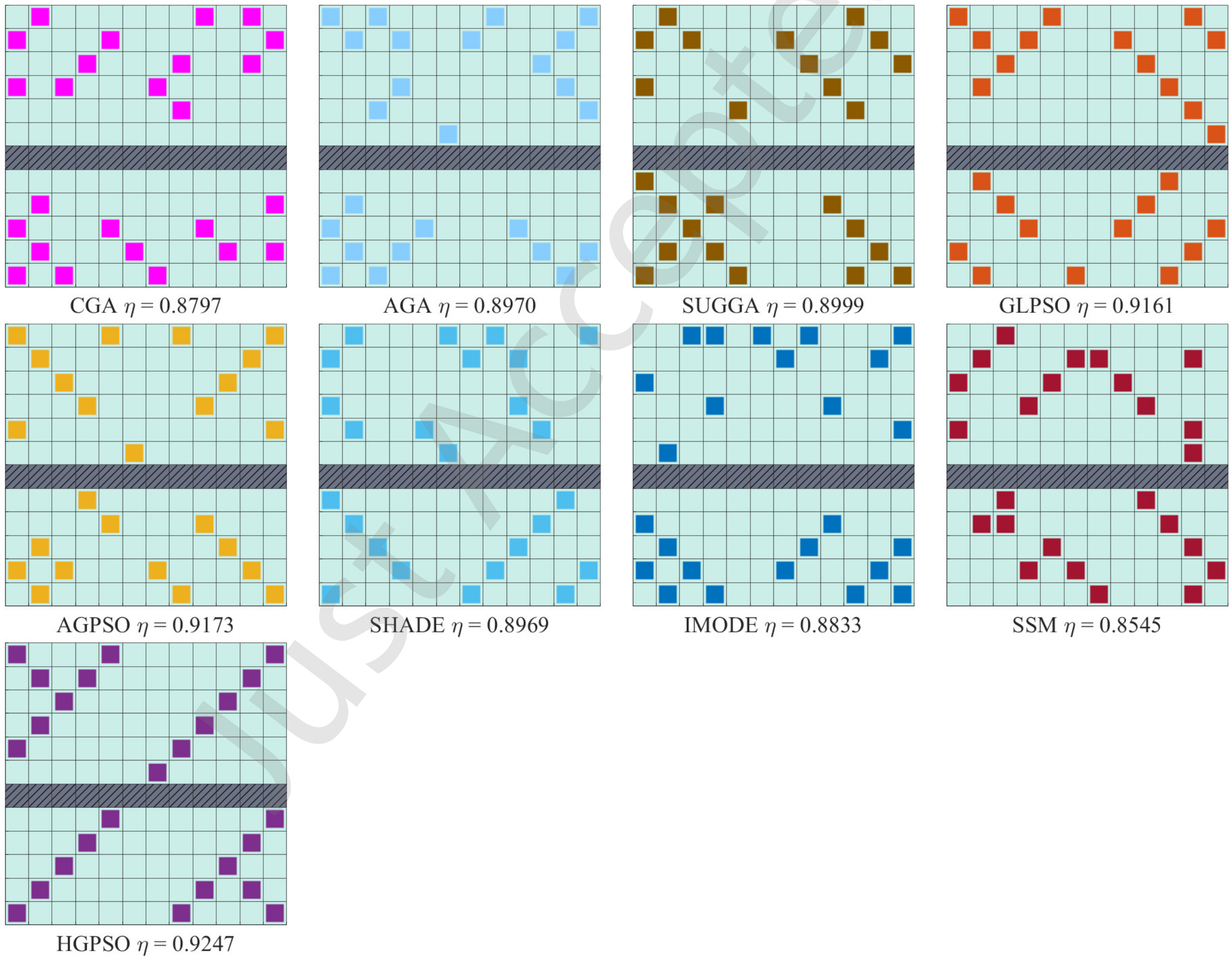

Fig. 21 The visualization of WFLOP solutions obtained from HGPSO and other competitors in wind scenario 4.

and the total runtime over k cycles is

$$O\Big(k \cdot NP \cdot (D + G + S\,D^2)\Big). \tag{29}$$

If the wake-evaluation routine is viewed as a black-box oracle and only the optimizer-side search steps are counted, the complexity reduces to $O(k \cdot NP \cdot D)$, which matches the population-dimension-iteration form often used to compare PSO-family optimizers. In the present WFLOP setting, however, the more transparent statement is that HGPSO scales

Table 13 Representative two-case sensitivity analysis of HGPSO under the same FE budget $maxFEs = 24000$ (3 independent runs per setting). Case A: WS2, 12×12, $N = 20$, constraint type 9. Case B: WS3, 12×12, $N = 25$, constraint type 12. For the replacement rule, the implementation uses $K = \lfloor r_w I_r I_c \rfloor + D$ candidate positions, capped by the total number of cells. In the last column, the effective ratios are reported as Case A / Case B.

Parameter	Value	Case A mean η (%)	Case A SD (%)	Case B mean η (%)	Case B SD (%)	Effective ratio A / B (%)
Acceleration coefficient c						
c	1.20	89.258	0.522	93.396	0.574	–
c	1.49618	89.718	0.080	93.282	0.057	–
c	1.80	89.674	0.374	93.461	0.235	–
Mutation rate p_m						
p_m	0.005	88.587	0.347	93.365	0.416	–
p_m	0.01	89.718	0.080	93.282	0.057	–
p_m	0.02	89.318	0.350	93.356	0.241	–
Branch threshold m						
m	0.80	89.237	0.292	93.305	0.274	–
m	0.90	89.718	0.080	93.282	0.057	–
m	0.95	89.385	0.405	93.446	1.048	–
Replacement-pool ratio r_w						
r_w	0.05	89.427	0.427	93.358	0.653	18.75/22.22
r_w	0.10	89.718	0.080	93.282	0.057	23.61/27.08
r_w	0.15	89.177	0.581	93.141	0.443	28.47/31.94
Population size NP						
NP	80	89.588	0.102	94.041	0.331	–
NP	120	89.653	0.298	93.757	1.002	–
NP	160	89.494	0.116	93.235	0.640	–

linearly with k and NP, while the main practical overhead is the wake-evaluation term.

A.3 Spacing-feasibility proof under grid encoding

Proposition 1. Any feasible layout $x \in \Omega$ produced by the repaired HGPSO encoding satisfies the minimum spacing requirement $d_{\min}$ between every pair of turbines.

Proof. Let $x = (x_1, \ldots, x_D) \in \Omega$ be a feasible HGPSO solution after repair, where each x_d is a valid grid index, all indices are distinct, and no index belongs to the restricted set CL. By construction of Ω, feasibility already excludes duplicate turbine indices, so any two turbines x_a and x_b with $a \neq b$ must occupy different grid cells. The encoding operator $E(\cdot)$ maps each valid index to the center of its grid cell. If two turbines occupy different cells, then their row-column differences $(\Delta r, \Delta c)$ are integers and cannot be simultaneously zero. Hence, the Euclidean distance between their encoded centers is

$$\|E(x_a) - E(x_b)\|_2 = W_t \sqrt{(\Delta r)^2 + (\Delta c)^2} \geqslant W_t. \tag{30}$$

In the benchmark platform used in this paper, $W_t = 231$ m, which equals three rotor diameters and therefore matches the required minimum spacing threshold $d_{\min}$. Consequently, any two distinct encoded turbines automatically satisfy $\|E(x_a) - E(x_b)\|_2 \geqslant d_{\min}$.

The subsequent rotation used in the wake model is a rigid orthogonal transformation. If R_θ is the rotation matrix for wind direction θ, then

$$\|R_\theta E(x_a) - R_\theta E(x_b)\|_2 = \|E(x_a) - E(x_b)\|_2. \tag{31}$$

Therefore, the coordinate rotation preserves all pairwise distances and cannot invalidate the spacing guarantee. This proves that the adopted grid encoding prevents spacing violations before wake evaluation and preserves that guarantee afterwards. □

A.4 Interpretation of the branch threshold m

Interpretation. The role of m can be interpreted through the expected prototype displacement before the final feasibility projection. Consider the informative case in which the current particle x_i^t, its reference exemplar e_i^t, and the global best x_g^t are not identical. Ignoring the later repair step for the moment, HGPSO selects one of two representative update branches:

$$\tilde{x}_i^{t+1} = \begin{cases} x_i^t + c\, r \odot (e_i^t - x_i^t), & \text{with probability } 1 - m, \\ e_i^t + c\, r \odot (x_g^t - e_i^t), & \text{with probability } m, \end{cases} \tag{32}$$

where $r \sim U([0,1]^D)$ and $\odot$ denotes element-wise multiplication. Using $\mathbb{E}[r] = \frac{1}{2}\mathbf{1}$, the expected pre-projection displacement is

$$\mathbb{E}\left[\tilde{x}_i^{t+1} - x_i^t\right] = (1-m)\frac{c}{2}(e_i^t - x_i^t) + m\left[(e_i^t - x_i^t) + \frac{c}{2}(x_g^t - e_i^t)\right]. \tag{33}$$

Define

$$\alpha(m) = \frac{c}{2} + m\left(1 - \frac{c}{2}\right), \qquad \beta(m) = m\frac{c}{2}, \tag{34}$$

so that

$$\mathbb{E}\left[\tilde{x}_i^{t+1} - x_i^t\right] = \alpha(m)(e_i^t - x_i^t) + \beta(m)(x_g^t - e_i^t). \tag{35}$$

Proposition 2. If $0 < c < 2$ and $m \in [0, 1]$, then $\alpha(m) > 0$, $\beta(m) \geqslant 0$, and the relay-to-local weight ratio

$$\rho(m) = \frac{\beta(m)}{\alpha(m)} = \frac{mc}{c + 2m - mc} \tag{36}$$

is strictly increasing in m.

Proof. For $0 < c < 2$, one has $1 - \frac{c}{2} > 0$, so $\alpha(m)$ increases linearly from $\frac{c}{2}$ at $m = 0$ to 1 at $m = 1$, and is therefore strictly positive on $[0, 1]$. Likewise, $\beta(m) = m\frac{c}{2} \geqslant 0$ and increases linearly with m. Differentiating $\rho(m)$ gives

$$\rho'(m) = \frac{c^2}{(c + 2m - mc)^2} > 0, \tag{37}$$

which proves that the relative weight assigned to the elite-relay direction increases monotonically with m. □

This expression shows that m continuously tunes the expected directional drift. A smaller m gives relatively more weight to direct local correction from x_i^t toward e_i^t, whereas a larger m strengthens the elite-relay path that moves first toward the exemplar level and then toward the global elite. In this sense, m acts as a probabilistic exploration–exploitation regulator in the surrogate continuous space from which the feasible discrete candidate is later projected. The interpretation is not presented as a strict global convergence proof; rather, it formalizes the directional bias induced by the branch mechanism and explains why the parameter has a clear optimization-theoretic meaning even in the repaired discrete search space.

Although the final HGPSO decision vector is repaired onto the discrete feasible set Ω, the above expectation remains useful because it explains the search bias induced before projection. Empirically, the representative sensitivity analysis in Table 13 shows that $m = 0.9$ provides the strongest overall compromise between mean performance and stability among the tested values. In Case A it attains both the highest mean and the smallest dispersion (89.718% ± 0.080%), whereas in Case B the nearby value $m = 0.95$ yields a slightly higher mean (93.446% versus 93.282%) at the cost of much larger variance (1.048% versus 0.057%). These results support the interpretation that a moderate-high elite-relay preference is beneficial for the considered WFLOP instances without justifying a more aggressive default threshold.

Declaration of competing interest

The authors have no competing interests to declare that are relevant to the content of this article.

Reference

[1] A. I. Osman, L. Chen, M. Yang, G. Msigwa, M. Farghali, S. Fawzy, D. W. Rooney, and P.-S. Yap, Cost, environmental impact, and resilience of renewable energy under a changing climate: a review, *Environmental Chemistry Letters*, vol. 21, no. 2, pp. 741–764, 2023.

[2] N. Maamoun, R. Kennedy, X. Jin, and J. Urpelainen, Identifying coal-fired power plants for early retirement, *Renewable and Sustainable Energy Reviews*, vol. 126, p. 109833, 2020.

[3] Y. Yang, P. E. Campana, and J. Yan, Potential of unsubsidized distributed solar pv to replace coal-fired power plants, and profits classification in chinese cities, *Renewable and Sustainable Energy Reviews*, vol. 131, p. 109967, 2020.

[4] A. Rahman, O. Farrok, and M. M. Haque, Environmental impact of renewable energy source based electrical power plants: Solar, wind, hydroelectric, biomass, geothermal, tidal, ocean, and osmotic, *Renewable and Sustainable Energy Reviews*, vol. 161, p. 112279, 2022.

[5] M. Farghali, A. I. Osman, K. Umetsu, and D. W. Rooney, Integration of biogas systems into a carbon zero and hydrogen economy: a review, *Environmental Chemistry Letters*, vol. 20, no. 5, pp. 2853–2927, 2022.

[6] S. Fawzy, A. I. Osman, J. Doran, and D. W. Rooney, Strategies for mitigation of climate change: a review, *Environmental Chemistry Letters*, vol. 18, pp. 2069–2094, 2020.

[7] M. S. Nazir, N. Ali, M. Bilal, and H. M. Iqbal, Potential environmental impacts of wind energy development: A global perspective, *Current Opinion in Environmental Science & Health*, vol. 13, pp. 85–90, 2020.

[8] P. Sorknæs, S. R. Djørup, H. Lund, and J. Z. Thellufsen, Quantifying the influence of wind power and photovoltaic on future electricity market prices, *Energy Conversion and Management*, vol. 180, pp. 312–324, 2019.

[9] X. Wang, L. Li, A. Palazoglu, N. H. El-Farra, and N. Shah, Optimization and control of offshore wind systems with energy storage, *Energy Conversion and Management*, vol. 173, pp. 426–437, 2018.

[10] L. Parada, C. Herrera, P. Flores, and V. Parada, Wind farm layout optimization using a gaussian-based wake model, *Renewable Energy*, vol. 107, pp. 531–541, 2017.

[11] S. Tao, S. Liu, R. Zhao, Y. Yang, H. Todo, and H. Yang, A state-of-the-art fractional order-driven differential evolution for wind farm layout optimization, *Mathematics*, vol. 13, no. 2, p. 282, 2025.

[12] J. Park and K. H. Law, Layout optimization for maximizing wind farm power production using sequential convex programming, *Applied Energy*, vol. 151, pp. 320–334, 2015.

[13] X. Ju and F. Liu, Wind farm layout optimization using self-informed genetic algorithm with information guided exploitation, *Applied Energy*, vol. 248, pp. 429–445, 2019.

[14] X. Ju, F. Liu, L. Wang, and W.-J. Lee, Wind farm layout optimization based on support vector regression guided genetic algorithm with consideration of participation among landowners, *Energy Conversion and Management*, vol. 196, pp. 1267–1281, 2019.

[15] R. Shakoor, M. Y. Hassan, A. Raheem, and Y.-K. Wu, Wake effect modeling: A review of wind farm layout optimization using jensen's model, *Renewable and Sustainable Energy Reviews*, vol. 58, pp. 1048–1059, 2016.

[16] G. Mosetti, C. Poloni, and B. Diviacco, Optimization of wind turbine positioning in large windfarms by means of a genetic algorithm, *Journal of Wind Engineering and Industrial Aerodynamics*, vol. 51, no. 1, pp. 105–116, 1994.

[17] S. Grady, M. Y. Hussaini, and M. M. Abdullah, Placement of wind turbines using genetic algorithms, *Renewable Energy*, vol. 30, no. 2, pp. 259–270, 2005.

[18] R. Archer, G. Nates, S. Donovan, and H. Waterer, Wind turbine interference in a wind farm layout optimization mixed integer linear programming model, *Wind Engineering*, vol. 35, no. 2, pp. 165–175, 2011.

[19] J. Park and K. H. Law, Layout optimization for maximizing wind farm power production using sequential convex programming, *Applied Energy*, vol. 151, pp. 320–334, 2015.

[20] M. Bilbao and E. Alba, Simulated annealing for optimization of wind farm annual profit, in *2009 2nd International Symposium on Logistics and Industrial Informatics*. IEEE, 2009, pp. 1–5.

[21] Y. Eroğlu and S. U. Seçkiner, Design of wind farm layout using ant colony algorithm, *Renewable Energy*, vol. 44, pp. 53–62, 2012.

[22] O. A. L. Brutto, S. S. Guillou, J. Thiébot, and H. Gualous, Assessing the effectiveness of a global optimum strategy within a tidal farm for power maximization, *Applied Energy*, vol. 204, pp. 653–666, 2017.

[23] S. Salcedo-Sanz, D. Gallo-Marazuela, A. Pastor-Sánchez, L. Carro-Calvo, A. Portilla-Figueras, and L. Prieto, Offshore wind farm design with the coral reefs optimization algorithm, *Renewable Energy*, vol. 63, pp. 109–115, 2014.

[24] J. Feng and W. Z. Shen, Design optimization of offshore wind farms with multiple types of wind turbines, *Applied Energy*, vol. 205, pp. 1283–1297, 2017.

[25] P. D. Pantula, N. K. Pujari, and K. Mitra, Handling wind stochasticity in farm layout optimization: A novel data-driven approach, in *Optimization, Uncertainty and Machine Learning in Wind Energy Conversion Systems*. Springer, 2025, pp. 153–172.

[26] Y. Du, X. Shen, B. Lu, and X. Ding, Joint optimization of layout and electrolyzer capacity for decentralized offshore wind-powered hydrogen production, *IEEE Transactions on Industrial Informatics*, 2025.

[27] T. Jard and R. Snaiki, Real-time dynamic layout optimization for floating offshore wind farm control, *Ocean Engineering*, vol. 316, p. 119971, 2025.

[28] Y. Wang, Y. Yang, S. Tao, L. Qi, and H. Shen, A reinforcement learning-assisted fractional-order differential evolution for

solving wind farm layout optimization problems, *Mathematics*, vol. 13, no. 18, p. 2935, 2025.

[29] L. Chen and E. MacDonald, Considering Landowner Participation in Wind Farm Layout Optimization, *Journal of Mechanical Design*, vol. 134, no. 8, p. 084506, 07 2012.

[30] Y. Chen, H. Li, K. Jin, and Q. Song, Wind farm layout optimization using genetic algorithm with different hub height wind turbines, *Energy Conversion and Management*, vol. 70, pp. 56–65, 2013.

[31] X. Gao, H. Yang, and L. Lu, Optimization of wind turbine layout position in a wind farm using a newly-developed two-dimensional wake model, *Applied Energy*, vol. 174, pp. 192–200, 2016.

[32] P.-Y. Yin, T.-H. Wu, and P.-Y. Hsu, Risk management of wind farm micro-siting using an enhanced genetic algorithm with simulation optimization, *Renewable Energy*, vol. 107, pp. 508–521, 2017.

[33] L. Parada, C. Herrera, P. Flores, and V. Parada, Wind farm layout optimization using a gaussian-based wake model, *Renewable Energy*, vol. 107, pp. 531–541, 2017.

[34] G. R. Scott and I. A. Johnston, Temperature during embryonic development has persistent effects on thermal acclimation capacity in zebrafish, *Proceedings of the National Academy of Sciences*, vol. 109, no. 35, pp. 14 247–14 252, 2012.

[35] L. G. Moore, Human genetic adaptation to high altitude, *High Altitude Medicine & Biology*, vol. 2, no. 2, pp. 257–279, 2001, pMID: 11443005.

[36] S. Tao, Y. Yang, R. Zhao, H. Todo, and Z. Tang, Competitive elimination improved differential evolution for wind farm layout optimization problems, *Mathematics*, vol. 12, no. 23, p. 3762, 2024.

[37] Z. Lei, S. Gao, Y. Wang, Y. Yu, and L. Guo, An adaptive replacement strategy-incorporated particle swarm optimizer for wind farm layout optimization, *Energy Conversion and Management*, vol. 269, p. 116174, 2022.

[38] X. Zhang, Q. Wang, S. Ye, K. Luo, and J. Fan, Efficient layout optimization of offshore wind farm based on load surrogate model and genetic algorithm, *Energy*, vol. 309, p. 133106, 2024.

[39] I. F. Da Silva, T. B. Lazzarin, L. Schmitz, and A. R. Panisson, Genetic algorithm-based optimization framework for offshore wind farm layout design, *IEEE Access*, 2025.

[40] S. Tao, R. Zhao, K. Wang, and S. Gao, An efficient reconstructed differential evolution variant by some of the current state-of-the-art strategies for solving single objective bound constrained problems, *arXiv preprint arXiv:2404.16280*, 2024.

[41] S. Tao, Y. Yang, R. Zhao, K. Wang, S. Liu, and S. Gao, Rdexsop: Exploitation-biased reconstructed differential evolution for fixed-budget bound-constrained single-objective optimization, *arXiv preprint arXiv:2603.27089*, 2026.

[42] Y.-J. Gong, J.-J. Li, Y. Zhou, Y. Li, H. S.-H. Chung, Y.-H. Shi, and J. Zhang, Genetic learning particle swarm optimization, *IEEE Transactions on Cybernetics*, vol. 46, no. 10, pp. 2277–2290, 2015.

[43] X. Yu, Z. Wu, H. Zhang, and Y. Li, Wind farm layout optimization through multi-strategy differential evolution-based reinforcement learning algorithm, *Energy*, p. 138221, 2025.

[44] D. H. Wolpert and W. G. Macready, No free lunch theorems for optimization, *IEEE Transactions on Evolutionary computation*, vol. 1, no. 1, pp. 67–82, 1997.

[45] Y. Wang, D. Song, F. Jurić, N. Duić, and H. Mikulčić, Multimodal optimization of offshore wind farm collection system topology based on nearest better most attractive particle swarm optimization, *Renewable and Sustainable Energy Reviews*, vol. 222, p. 115978, 2025.

[46] L. Shen, P. Zhou, Y. Han, L. Mi, W. Xu, and J. Xu, Wind farm layout optimization based on dynamic levy sparrow search algorithm: A multi-parameter analysis with active yaw control, *Energy*, vol. 324, p. 135989, 2025.

[47] Y. Zhang, Z. Zhang, R. Zhong, J. Yu, E. H. Houssein, J. Zhao, and Z. Gao, Under complex wind scenarios: Considering large-scale wind turbines in wind farm layout optimization via self-adaptive optimal fractional-order guided differential evolution, *Energy*, vol. 323, p. 135866, 2025.

[48] N. O. Jensen, *A note on wind generator interaction*, ser. Risø-M. Risø National Laboratory, 1983, no. 2411.

[49] B. L. Du Pont and J. Cagan, An Extended Pattern Search Approach to Wind Farm Layout Optimization, *Journal of Mechanical Design*, vol. 134, no. 8, p. 081002, 07 2012.

[50] R. Tanabe and A. Fukunaga, Success-history based parameter adaptation for differential evolution, in *2013 IEEE Congress on Evolutionary Computation*. IEEE, 2013, pp. 71–78.

[51] K. M. Sallam, S. M. Elsayed, R. K. Chakrabortty, and M. J. Ryan, Improved multi-operator differential evolution algorithm for solving unconstrained problems, in *2020 IEEE Congress on Evolutionary Computation (CEC)*. IEEE, 2020, pp. 1–8.

[52] S. Tao, K. Wang, T. Jin, Z. Wu, Z. Lei, and S. Gao, Spherical search algorithm with memory-guided population stage-wise control for bound-constrained global optimization problems, *Applied Soft Computing*, p. 111677, 2024.

[53] S. Gao, K. Wang, S. Tao, T. Jin, H. Dai, and J. Cheng, A state-of-the-art differential evolution algorithm for parameter estimation of solar photovoltaic models, *Energy Conversion and Management*, vol. 230, p. 113784, 2021.

[54] E. A. Gehan, A generalized wilcoxon test for comparing arbitrarily singly-censored samples, *Biometrika*, vol. 52, no. 1-2, pp. 203–224, 1965.

[55] J. Carrasco, S. García, M. Rueda, S. Das, and F. Herrera, Recent trends in the use of statistical tests for comparing swarm and evolutionary computing algorithms: Practical guidelines and a critical review, *Swarm and Evolutionary Computation*, vol. 54, p. 100665, 2020.

[56] A. Cully and Y. Demiris, Quality and diversity optimization: A unifying modular framework, *IEEE Transactions on Evolutionary Computation*, vol. 22, no. 2, pp. 245–259, 2017.

Author biography

Tao Zheng received the M.E. degree from the University of Toyama, Toyama, Japan, in 2023, where he is currently pursuing the Ph.D. degree. His research interests include computational intelligence and neural networks, with a particular focus on evolutionary computation and brain-inspired learning models. His current research primarily focuses on intelligent evolutionary algorithms for complex optimization problems.

Sichen Tao received the B.E. degree from the University of Shanghai for Science and Technology, China, and the Ph.D. degree in Engineering from the University of Toyama, Japan, in 2025. He is currently an Assistant Professor with the Cyberscience Center, Tohoku University, Japan. His research interests include artificial intelligence (AI), with a focus on machine learning, deep learning, reinforcement learning, brain-inspired neural networks, computational intelligence, and optimization. His application areas include high-performance computing (HPC), disaster prevention and mitigation, new energy, Industry 5.0, autonomous driving, human–robot collaboration systems, healthcare, and AI & HPC for scientific discovery.

Wenzhu Gu received the B.S. degree in English from Jiangsu Normal University, Jiangsu, China, in 2014. She is currently pursuing the M.S. degree at the Faculty of Engineering, University of Toyama, Japan. Her current research interests include evolutionary computation and machine learning.

Zhenyu Lei received the Ph.D. degree in Science and Engineering from the University of Toyama, Toyama, Japan, in 2023. He is currently an Assistant Professor at the Faculty of Engineering, University of Toyama, Japan. His current research interests include evolutionary computation, machine learning, and neural networks for real-world applications and optimization problems.

Shangce Gao received his Ph.D. degree in Innovative Life Science from the University of Toyama, Toyama, Japan, in 2011. He is currently a Professor with the Faculty of Engineering at the University of Toyama. His research interests focus on brain-inspired neural networks and their applications in medical diagnosis and drug discovery. He serves as an Associate Editor for several international journals, including IEEE Transactions on Neural Networks and Learning Systems and the IEEE/CAA Journal of Automatica Sinica.

— end unify —